

Acoustic scattering in a duct with mean swirling flow

By C. J. HEATON AND N. PEAKE

Department of Applied Mathematics and Theoretical Physics, University of Cambridge,
Wilberforce Road, Cambridge CB3 0WA, UK

(Received 19 January 2005 and in revised form 25 April 2005)

In this paper we consider the diffraction of waves by a sharp edge in three-dimensional flow with non-zero mean vorticity. This is an extension of the famous Sommerfeld problem of the diffraction of waves by a sharp edge in quiescent conditions. The precise problem concerns an infinitely long annular circular cylinder, which contains a concentric semi-infinite circular cylinder which acts as a splitter. The mean flow has both axial and swirl components, and cases in which the splitter is arranged with either a leading edge or a trailing edge relative to the axial flow are considered. This is a model of a number of practical situations in the aeroengine context. We treat both sonic and nearly-convected incident disturbances, and two regimes are considered; one in which the azimuthal order, m , of the incident waves is $O(1)$, and a second in which $m \gg 1$. A solution for $m = O(1)$ in the case of rigid-body swirl is found using the Wiener–Hopf technique, and special care is needed to handle the infinite accumulation of scattered nearly-convected modes which results from the presence of the mean vorticity. Simplification in the limit $m \gg 1$ then allows us to consider more general swirl distributions. A number of effects arise due to the presence of mean vorticity. This includes the generation of sound at a trailing edge due to the scattering of a nearly-convected disturbance, which is to be contrasted with the way in which a convected gust passes a trailing edge silently in uniform mean flow.

1. Introduction

Problems of wave scattering by rigid surfaces are of considerable interest in acoustics. One of the most famous canonical problems in wave theory is due to Sommerfeld and concerns the diffraction of a wave by a sharp edge, with the disturbance field satisfying the simple scalar Helmholtz equation with rigid boundary conditions on the semi-infinite plate. A range of extensions to this problem have been completed over the years, but we mention in particular here extensions in two distinct directions. First, Goldstein (1978*a*, 1979) considered the edge to be embedded in an infinite two-dimensional parallel shear flow. Second, Rawlins (1995) considered the three-dimensional axisymmetric problem of sound radiation from a semi-infinite cylinder inside a co-axial infinite cylinder, in zero flow. Related to this, the trifurcated-waveguide problem with wall lining in two dimensions was considered by Mahmoud-Ul-Hassan & Rawlins (1999), and with uniform mean flow by Mahmoud-Ul-Hassan & Rawlins (1998). In this paper we seek to combine these approaches by considering several scattering problems in the geometry of a cylindrical duct carrying vortical mean flow.

The precise problem we consider concerns an infinitely long annular circular cylinder, which contains a concentric semi-infinite circular cylinder which acts as a splitter (see figure 1). The mean flow has both axial and swirl components, and cases in which the splitter is arranged with either a leading edge or a trailing edge relative to the axial flow are considered. This is a model of a number of practical situations in the aeroengine context. For instance, the inter-stage region between the fan and the outlet guide vanes bifurcates into the engine core (inner) and bypass-duct (outer) flows. Here one is interested in the way in which engine core noise is diffracted at this bifurcation, and might therefore escape to the far field via the bypass duct. Since the mean flow in this region is strongly swirling, the inclusion of the effects of mean vorticity is an important feature of our model. Another possible application, this time in which the lip of the bifurcation acts as a trailing edge, is to coaxial injectors in combustion system, where mean swirl may be included to enhance mixing.

The presence of mean vorticity couples the familiar, and otherwise uncoupled, acoustic and vorticity modes of a fluid system. Instead of two distinct mode types, one irrotational, the other incompressible and with zero pressure (i.e. noiseless), we have a single spectrum which contains two distinct families of modes. Analogously termed *sonic* and *nearly-convected*, the former have small vorticity and the latter small divergence and pressure. Early work on the modes of swirling flow in a duct was completed by Kerrebrock (1977), and more recently by Golubev & Atassi (1998) and Tam & Auriault (1998). The flow considered in these papers, and also here, is one with mean axial and swirling (azimuthal) velocity components which depend only on the radial coordinate r . In general, finding the combined spectrum of acoustic–vorticity modes for such a problem is difficult. In particular, after Fourier decomposing the unsteady small perturbation in axial coordinate x and time t , and assuming fixed azimuthal mode order (i.e. unsteady perturbation proportional to $\exp(im\theta)$, with θ the azimuthal angle) the resulting ordinary differential equation in r has a singular point, or *critical layer*. The critical layer occurs precisely where the convected derivative with respect to the mean flow vanishes and, given the r dependence of the mean flow, exists for a range of axial wavenumbers, k . This implies that there is a branch cut in the Fourier transform of the disturbance or, equivalently, a continuous portion of the eigenvalue spectrum of k -wavenumbers. Another complication associated with the critical layer is that we tend to see clustering of discrete k -modes at the ends of the continuous portion of the spectrum. Indeed, an accumulation of infinitely many modes can occur, which is difficult to analyse or compute numerically. Examples of several calculated spectra of acoustic–vorticity modes showing these features, and also the sonic modes, are given by Golubev & Atassi (1998). The difficulty in resolving the eigenmodes and eigenvalues with sufficient accuracy in the nearly-convected part of the spectrum is such that some recent work has instead looked at the axial development of the flow from the point of view of an initial-value problem, see for instance Golubev & Atassi (2000) and Cooper & Peake (2005). In this paper we first consider the case in which the axial mean flow is uniform and the swirl is solid-body rotation. In this case the continuous spectrum is degenerate and reduces to a single point, and the nearly-convected spectrum is composed of an infinity of discrete modes which accumulate towards the wavenumber of pure convection. We then use asymptotic analysis in the (practically realistic) limit of large m , together with the initial-value approach mentioned above, to cover cases with more general mean flows.

The Wiener–Hopf technique is employed to obtain solutions to the various scattering problems in the form of a modal description of the scattered field. The infinite tails

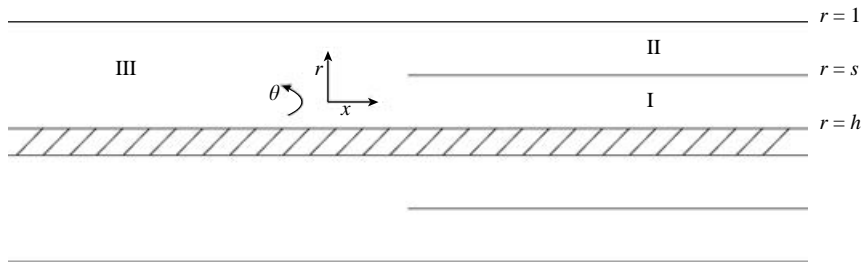


FIGURE 1. The geometry of the annular axisymmetric duct and splitter. The mean flow has an axial component (from left to right in the leading-edge configuration considered in §2.3), plus a swirling (azimuthal) component.

of the nearly-convected and sonic parts of the spectrum are considered carefully, which then allows truncation of the resulting infinite sums of modal contributions and easy computation. In particular, the amplitudes of the cut-on waves propagating away from the edge can be found with very little effort. An alternative approach has been used by Nijboer (2003), who neglects the nearly-convected part of the spectrum and performs mode matching on the sonic modes. Nijboer expands the scattered field in terms of a large number of sonic modes in each of the three regions, and the unknown amplitudes are determined by insisting that pressure and velocity are suitably continuous across the edge cross-sectional plane $x = 0$. We will see that for the scattering of sound waves at a leading edge, and provided that the azimuthal order m is large, neglect of the nearly-convected part of the spectrum is reasonable. However, for more general cases, involving incident nearly-convected disturbances, or scattering by a trailing edge, or for $m = O(1)$, the sort of exact (§§2,3) or rational-asymptotic (§4) analysis we present here is required.

The remainder of this paper is set out as follows. In §2 the modal structure in an infinite duct for rigid-body swirl is reviewed, and the solution for scattering by a leading-edge geometry is presented. In §3 we repeat this analysis for a trailing-edge geometry. In §4 we then go on to consider the large- m limit for a more general mean flow; the necessary results from Cooper & Peake (2005) are reviewed, and we then consider scattering of sonic and nearly-convected disturbances by leading and trailing edges. Concluding remarks are presented in §5.

2. Scattering at a leading edge in rigid-body swirl

2.1. Formulation of problem

The geometry of the flow is shown in figure 1, and comprises an axisymmetric annular cylindrical duct $h \leq r \leq 1$ of infinite length, with r the radial coordinate, and with a coaxial semi-infinite rigid splitter of zero thickness on $r = s$, $x > 0$ (with x the axial coordinate). Throughout lengths are non-dimensionalized by the outer radius of the duct, densities by the mean density at $r = 1$, and velocities by the speed of sound at $r = 1$. The total fluid velocity, \mathbf{U}_{tot} , has the form of a uniform axial plus solid-body swirl mean flow with a small-amplitude unsteady disturbance,

$$\mathbf{U}_{tot}(x, r, \theta, t) = \mathbf{U}_0(r) + \mathbf{u}'(x, r, \theta, t) \quad (2.1)$$

where $\mathbf{U}_0(r) = Ue_x + \Omega r e_\theta$, θ is the azimuthal angle and t is the non-dimensional time. We assume that the mean flow and the perturbation are homentropic.

The disturbance field is decomposed in the way proposed by Goldstein (1978*b*) as

$$\mathbf{u}' = \mathbf{u} + \nabla\phi, \quad (2.2)$$

and the unsteady potential ϕ is chosen so that the unsteady pressure, p' , is given solely in terms of ϕ , i.e.

$$p' = -\rho_0 \frac{D_0\phi}{Dt}, \quad (2.3)$$

where ρ_0 is the local mean density and D_0/Dt is the mean-flow Lagrangian derivative. The equations of momentum and mass conservation then become

$$\frac{D_0\mathbf{u}}{Dt} + \mathbf{u} \cdot \nabla U_0 = -\xi_0 \wedge \nabla\phi, \quad (2.4)$$

$$\frac{D_0}{Dt} \frac{1}{c_0^2} \frac{D_0\phi}{Dt} - \frac{1}{\rho_0} \nabla \cdot (\rho_0 \nabla\phi) = \frac{1}{\rho_0} \nabla \cdot (\rho_0 \mathbf{u}) \quad (2.5)$$

respectively, where $\xi_0 = 2\Omega \mathbf{e}_x$ is the vorticity of the mean flow. The boundary conditions for (2.4) and (2.5) are zero normal (i.e. radial) flow on all the walls, together with the requirements of continuity of pressure throughout the fluid and outgoing scattered waves upstream and downstream. It is clear that the presence of mean vorticity, $\xi_0 \neq 0$, couples the two portions of the unsteady velocity together, so that in particular the unsteady vorticity is coupled to the unsteady pressure.

2.2. Duct modes

Before considering the semi-infinite geometry described in figure 1, we must first seek a modal solution to the problem of an infinite annular duct with rigid inner and outer walls at (for generality) $r = \sigma, t$. We therefore write

$$\phi = \phi(r) e^{ikx + im\theta - i\omega t}, \quad \mathbf{u} = \mathbf{u}(r) e^{ikx + im\theta - i\omega t}, \quad (2.6)$$

and we will suppose that the frequency ω and the azimuthal mode order m are given, while the axial wavenumber k will be found below as the solution of an eigenvalue problem. After some manipulation of (2.4) and (2.5), the mode-shape equation in this case is found to be

$$\left[\phi'' + \left(\frac{1}{r} + \frac{\Omega^2 r}{c_0^2} \right) \phi' - \frac{m^2}{r^2} \phi \right] \frac{\Lambda^2}{\Lambda^2 - 4\Omega^2} + \left[\frac{\Lambda^2}{c_0^2} - k^2 + \frac{2m\Omega^3 \Lambda}{c_0^2(\Lambda^2 - 4\Omega^2)} \right] \phi = 0, \quad (2.7)$$

where the prime denotes differentiation with respect to r . The mean local sound speed, $c_0(r)$, is given by

$$c_0^2 = 1 + (\gamma - 1)\Omega^2(r^2 - 1)/2, \quad (2.8)$$

where γ is the ratio of specific heats and

$$\Lambda(k) = kU - \omega + m\Omega \equiv U(k - k_c) \quad (2.9)$$

corresponds to the convective operator D_0/Dt , with k_c the convected wavenumber for which $\Lambda = 0$. We note in passing that (2.7) is an example of Keldysh polynomial operator pencils, see Yakubov (1994) for a pure-mathematical discussion. Note that Λ and k_c are independent of r for uniform axial flow with rigid-body swirl, and so there is no single critical radius at which the coefficient of the highest derivative in (2.7) vanishes. The only possible singular point of (2.7) occurs for pure convection, $k = k_c$, for which the coefficient of the highest derivative term ϕ'' vanishes for all r . In this case the equations need to be treated with a little care. However, by combining the

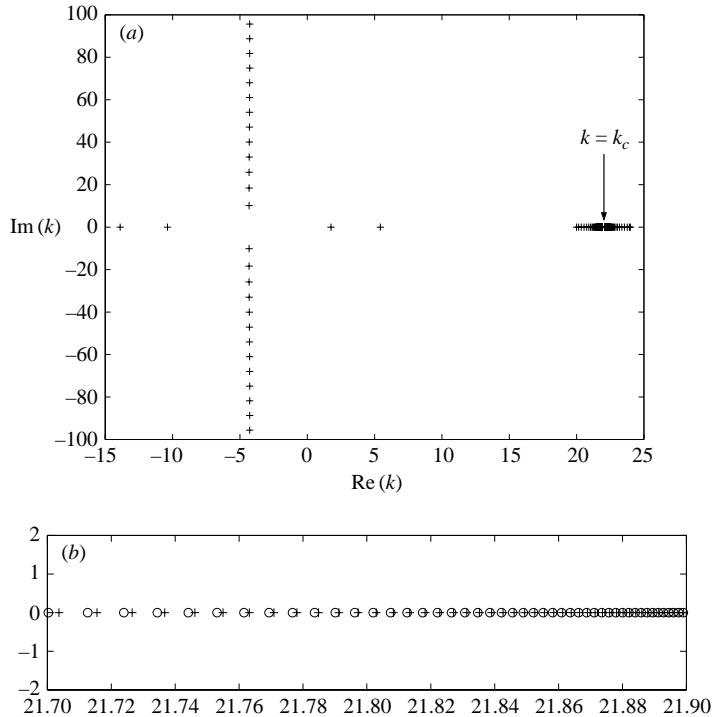


FIGURE 2. (a) A typical axial wavenumber spectrum for $\Omega = 0.4, U = 0.4, \omega = 10, m = 3$ with duct $0.5 \leq r \leq 1$ and (b) a close-up near $k = k_c$. Cross symbols represent exact numerical values and circles represent the asymptotic eigenvalues given by (2.11). For the modes shown n ranges from 23 to 70.

equations of mass and momentum conservation and setting $k = k_c$ we find that a non-zero exactly convected disturbance is only possible in the special case $\omega = m\Omega, k = 0$, or when $\Omega = 0$ (this latter point will be important when considering the existence or otherwise of a wake sheet downstream of a trailing edge, see §3). In general, the total unsteady velocity and unsteady pressure associated with the $k = k_c$ mode are zero.

The boundary condition of zero radial velocity on the hard walls becomes

$$u_r + \frac{\partial \phi}{\partial r} = \frac{\Lambda (\Lambda \phi' + 2\Omega m \phi / r)}{\Lambda^2 - 4\Omega^2} = 0 \quad \text{on} \quad r = \sigma, t. \quad (2.10)$$

The nonlinear dependence of (2.7) on the eigenvalue, k , signifies that this is not a Sturm–Liouville eigenvalue problem, and one consequence of this is that the eigenmodes are not orthogonal. We will return to this point in §5. Equation (2.7) with boundary condition (2.10) is integrated numerically using a standard variable-step-size routine. The eigenvalue was found by shooting, starting from the inner wall and then varying k until the boundary condition on the outer wall is satisfied. A typical eigenvalue spectrum is shown in figure 2(a). It is composed of a sonic family (analogous to the acoustic modes of uniform flow) of which four are cut-on and an infinite number are cut-off, and a nearly-convected family comprising an infinite number of discrete neutral modes which cluster on either side of the convected wavenumber $k = k_c$ (in uniform flow these nearly-convected modes all collapse onto the point of pure convection).

For the scattering problems to be considered later, we will need an analytical description of both the modes close to $k = k_c$ and the high-order cut-off sonic modes. Turning first to the nearly-convected modes, for $0 < \Lambda^2 \ll 1$ we can perform a multiple scales analysis similar to that of Golubev & Atassi (1998), and standard methods yield expressions for the wavenumbers and the mode shapes. After some algebra, it follows that the axial eigenvalues close to $k = k_c$ are

$$k - k_c = \frac{2\Omega k_c(t - \sigma)}{Un\pi} \left(1 - \frac{R(t, \sigma)}{n\pi} \right) + O(1/n^3), \quad (2.11)$$

where n is an integer labelling the modes (with $n > 0$ and $n < 0$ corresponding to $k > k_c$ and $k < k_c$ respectively, and $|n|$ increasing corresponding to moving closer to $\Lambda = 0$), and

$$R(t, \sigma) = -\tan^{-1} \left(\frac{mk_c(t - \sigma)}{m^2 + \sigma tk_c^2} \right) - \frac{m}{k_c(\gamma - 1)\alpha} \tan^{-1} \left(\frac{t - \sigma}{\alpha + \sigma t/\alpha} \right) - \frac{2\Omega(t - \sigma)}{U} \quad (2.12)$$

where $\alpha^2 = 2/\{(\gamma - 1)\Omega^2\} - 1$. The corresponding eigenfunction mode shape is

$$\phi(r) = \frac{1}{\sqrt{r\rho_0(r)}} \sin \left(\frac{n\pi r}{t - \sigma} + \psi_0 \right) + O(1/n), \quad (2.13)$$

where the complicated expression for the $O(1)$ phase shift ψ_0 has been obtained but is omitted for brevity. Figure 2(b) shows a close-up of the clustering near k_c , with good agreement between the numerical and asymptotic eigenvalues as the convected wavenumber is approached. Good agreement between numerical and asymptotic mode shapes has also been found.

Turning now to the infinite cut-off tails of the sonic part of the spectrum, a WKB solution for large $|k|$ can be used to obtain leading-order expressions for these eigenvalues in the form

$$k = an + b + O(n^{-1}), \quad (2.14)$$

where $n \rightarrow \pm\infty$ is an integer labelling the modes in the upper/lower half-planes respectively. For the more general mean flow $U_0(r) = U_x(r)\mathbf{e}_x + U_\theta(r)\mathbf{e}_\theta$ to be used in §4, of which the current mean flow is a special case, we find

$$a = i\pi \left(\int_\sigma^t \sqrt{1 - U_x^2(r)/c_0^2(r)} \, dr \right)^{-1}, \quad (2.15)$$

$$b = a \left(\frac{1}{i\pi} \int_\sigma^t \frac{U_x(mU_\theta/r - \omega)}{c_0^2 \sqrt{1 - U_x^2/c_0^2}} \, dr - n_3^\pm \right), \quad (2.16)$$

where n_3^\pm are integers which simply shift the index of the infinite sequences and are determined by, for example, choosing to start counting the sonic eigenvalues from $n = \pm 1$. Expressions for the corresponding eigenmodes have also been determined, and in all cases good agreement has been found with numerically determined values.

In what follows the eigenvalues and eigenmodes of the infinite ducts are labelled by μ , the entire spectrum corresponding to the set of labels S , say. We also define some subsets of S for convenience: let S_a^+ correspond to the downstream modes in the sonic part of the spectrum (i.e. cut-on modes propagating downstream and an infinite tail of evanescent waves which decay in the downstream direction); S_a^- to the upstream modes in the sonic part of the spectrum; and S_c to the nearly-convected portion of the spectrum (which has two infinite tails near $k = k_c$, which all propagate downstream). It follows that $S = S_a^+ \cup S_a^- \cup S_c$.

In summary, we have presented an analytical description of the infinite tails of both the nearly-convected and sonic parts of the spectrum, and this will be crucial in the next subsection when we come to sum the contributions from these modes.

2.3. The Wiener–Hopf problem

We now wish to apply the Wiener–Hopf technique (see Noble 1958) to the problem of the scattering of unsteady flow by the leading edge of the splitter plate $r = s$ as seen in figure 1. We begin by writing the unsteady potential, for given ω and m , in the form

$$\phi = \psi_{tot}(x, r)e^{im\theta - i\omega t}. \quad (2.17)$$

The full-range Fourier transform in the x -direction is defined by

$$\hat{f}(\alpha) = \int_{-\infty}^{\infty} f(x)e^{-i\alpha x} dx, \quad (2.18)$$

and then the transform $\hat{\psi}_{tot}(k, r)$ satisfies (2.7). We write the total unsteady potential as the sum of a given incident component, ψ_{inc} , and a scattered component, ψ , so that $\psi_{tot} = \psi + \psi_{inc}$, and in order to cover all possible forms of incident field (i.e. acoustic waves from upstream or downstream, or nearly-convected waves from upstream) we write $\psi_{inc} = R + L$, where R are right-running eigenmodes incident from region III (i.e. upstream, see figure 1), and L are left-running eigenmodes incident from regions I or II (i.e. downstream).

The boundary conditions are zero radial flow on the duct walls and on the splitter, while within the fluid the pressure and velocity are continuous. In particular, the conditions at the splitter radius are that

$$(\mathbf{u} + \nabla\phi) \cdot \mathbf{e}_r = 0 \quad \text{on} \quad r = s, x > 0, \quad (2.19)$$

and that p' is continuous across $r = s, x < 0$. Also there is the causality/radiation condition that ψ is composed of outgoing waves at infinity. This latter condition will be satisfied by introducing a small fictitious dissipation, $0 < \text{Im}(\omega) \ll 1$, as is standard in Wiener–Hopf problems, which can then be set to zero at the end of the analysis. Note that this rigid-body flow is stable for all values of U, Ω , as follows directly from equation (3.6) of Lalas (1975).

To start, we let $Q_h(r, k)$ and $Q_t(r, k)$ be the solutions of (2.7) which satisfy the zero-radial-velocity condition (2.10) such that

$$(\Lambda(k)\partial/\partial r + 2\Omega m/r)Q = 0 \quad (2.20)$$

at $r = h, 1$ respectively, but with the right-hand side of (2.20) equal to 1 at $r = s$ in both cases. Note that $Q_{h,t}$ must be evaluated numerically, and closed-form solutions are not available. By using (2.20) and the fact that the radial velocity is continuous everywhere (including across the splitter, where it is zero) we find

$$\hat{\psi}(r, k) = \begin{cases} A(k)Q_h(r, k), & h < r < s \\ A(k)Q_t(r, k), & s < r < 1 \end{cases} \quad (2.21)$$

for some unknown $A(k)$. Fourier transforming (2.19), gives

$$0 = A(k) \frac{\Lambda(k)}{\Lambda(k)^2 - 4\Omega^2} - F_+(k) + R_-(k), \quad (2.22)$$

where $R_-(k)$ is a half-range Fourier transform of the radial velocity of the incident field on $r = s$,

$$R_-(k) = \int_0^\infty e^{-ikx} (\mathbf{u}_{inc} + \nabla\phi_{inc}) \cdot \mathbf{e}_r|_{r=s} dx, \quad (2.23)$$

and $F_+(k)$ is a half-range Fourier transform of the radial velocity of the scattered field on $r = s$,

$$F_+(k) = \int_{-\infty}^0 e^{-ikx} (\mathbf{u} + \nabla\phi) \cdot \mathbf{e}_r|_{r=s} dx. \quad (2.24)$$

The condition of continuity of pressure across $r = s$ for $x < 0$ gives

$$0 = \Lambda(k)A(k) (Q_t(s, k) - Q_h(s, k)) - P_-(k) + L_+(k), \quad (2.25)$$

where

$$L_+(k) = \int_{-\infty}^0 e^{-ikx} \Lambda \left(-i \frac{\partial}{\partial x} \right) [L(x, s)]_+^\pm dx, \quad (2.26)$$

$$P_-(k) = \int_0^\infty e^{-ikx} \Lambda \left(-i \frac{\partial}{\partial x} \right) [\psi(x, s)]_-^\pm dx. \quad (2.27)$$

The square brackets notation used in (2.26) and (2.27), and below, denotes the jump value

$$[\psi(x, s)]_-^\pm = \lim_{\epsilon \rightarrow 0^+} \psi(x, s + \epsilon) - \psi(x, s - \epsilon). \quad (2.28)$$

The quantities $R_-(k)$ and $L_+(k)$ depend only on the incident field, and are known, while $F_+(k)$ and $P_-(k)$ refer to the normal velocity upstream and the pressure jump downstream of the scattered field on $r = s$, and are at this stage unknown.

We define the Wiener–Hopf kernel by

$$K(k) = Q_t(s, k) - Q_h(s, k) \equiv K_+(k)K_-(k). \quad (2.29)$$

Note that no closed-form expression is available for $K(k)$, since equation (2.7) can only be solved numerically, although an infinite-product representation is possible (see Appendix A). The notation used in (2.22)–(2.29) is that subscripts \pm denote a function which is holomorphic (analytic) in the upper half- k -plane (UHP) or lower half- k -plane (LHP) respectively. Furthermore, in (2.29) we insist that the factors $K_\pm(k)$ are non-zero and possess algebraic behaviour at infinity in the UHP and LHP respectively. Full details of the way in which this factorization is completed are given in Appendix A. Since the frequency is supposed to have a small positive imaginary part, there is a strip containing the real- k -axis, $|\text{Im}(k)| < \delta$ say, in which all quantities are holomorphic, and the UHP/LHP correspond to $\text{Im}(k) > -\delta$ and $\text{Im}(k) < \delta$ respectively.

In the previous subsection we described the spectrum of axial wavenumbers allowed in a cylindrical duct $\sigma \leq r \leq t$, and with suitable choice of σ, t these results are now applied to the regions I, II and III. The incident field will be written as a modal decomposition, with vector \mathbf{B} of given modal amplitudes. So for instance, if we consider a field incident from region III upstream the incident field is

$$R = \sum_{\mu \in S_d^+ \cup S_c} B_{3\mu} U_{3\mu}^{(+)}(r) e^{i\alpha_{3\mu}^+ x}, \quad (2.30)$$

where the $\alpha_{3\mu}^+$ and $U_{3\mu}^{(+)}(r)$ are the eigenvalues and corresponding eigenfunctions for the duct modes in region III. These eigenvalues satisfy $K(\alpha_{3\mu}^+) = 0$, and the + superscript here means that they are located in the UHP. The sum (2.30) has contributions to R from, potentially, both the nearly-convected and sonic modes. A suitable normalization for the mode shapes can be chosen, for instance in our calculations we choose to normalize to unity the integral of $|U(r)|^2$, but the exact choice of normalization is unimportant because the whole problem is linear. In the same way, for incident modes propagating from downstream, the incident field can be written

$$L = \begin{cases} \sum_{\mu \in S_a^-} B_{1\mu} U_{1\mu}^{(-)}(r) e^{i\alpha_{1\mu}^- x}, & h < r < s \\ \sum_{\mu \in S_a^-} B_{2\mu} U_{2\mu}^{(-)}(r) e^{i\alpha_{2\mu}^- x}, & s < r < 1. \end{cases} \quad (2.31)$$

The eigenvalues $k = \alpha_{1\mu}$ of region I are poles of $Q_h(s, k)$, and the eigenvalues $k = \alpha_{2\mu}$ of region II are poles of $Q_l(s, k)$.

We now proceed to derive the Wiener–Hopf equation. After eliminating $A(k)$ between (2.22) and (2.25) and noting that k_c lies in the UHP, we introduce the quantity

$$D(\alpha_{3\mu}^\pm) \equiv \Lambda(\alpha_{3\mu}^\pm) U_{3\mu}^{(\pm)'}(s) + 2\Omega m U_{3\mu}^{(\pm)}(s)/s, \quad (2.32)$$

and group the functions K , K_\pm , D , and Λ in round brackets with a single argument to simplify notation (for instance, we write $(K_- \Lambda)_k$ for $K_-(k)\Lambda(k)$). With this convention the Wiener–Hopf equation becomes

$$\begin{aligned} & F_+(k)K_+(k) - R_-(k)K_+(k) - i \sum_{\mu \in S_a^+ \cup S_c} \frac{B_{3\mu}}{k - \alpha_{3\mu}^+} \left(\frac{\Lambda D K_+}{\Lambda^2 - 4\Omega^2} \right)_{\alpha_{3\mu}^+} \\ & - i \sum_{\mu \in S_a^-} \frac{B_{1\mu} U_{1\mu}^-(s)}{k - \alpha_{1\mu}^-} \left(\frac{\Lambda}{K_-(\Lambda^2 - 4\Omega^2)} \right)_{\alpha_{1\mu}^-} + i \sum_{\mu \in S_a^-} \frac{B_{2\mu} U_{2\mu}^-(s)}{k - \alpha_{2\mu}^-} \left(\frac{\Lambda}{K_-(\Lambda^2 - 4\Omega^2)} \right)_{\alpha_{2\mu}^-} \\ & = \frac{P_-(k)}{(K_-(\Lambda^2 - 4\Omega^2))_k} - \frac{L_+(k)}{(K_-(\Lambda^2 - 4\Omega^2))_k} - i \sum_{\mu \in S_a^+ \cup S_c} \frac{B_{3\mu}}{k - \alpha_{3\mu}^+} \left(\frac{\Lambda D K_+}{\Lambda^2 - 4\Omega^2} \right)_{\alpha_{3\mu}^+} \\ & - i \sum_{\mu \in S_a^-} \frac{B_{1\mu} U_{1\mu}^-(s)}{k - \alpha_{1\mu}^-} \left(\frac{\Lambda}{K_-(\Lambda^2 - 4\Omega^2)} \right)_{\alpha_{1\mu}^-} + i \sum_{\mu \in S_a^-} \frac{B_{2\mu} U_{2\mu}^-(s)}{k - \alpha_{2\mu}^-} \left(\frac{\Lambda}{K_-(\Lambda^2 - 4\Omega^2)} \right)_{\alpha_{2\mu}^-}. \end{aligned} \quad (2.33)$$

As usual, the two sides of the equation are respectively holomorphic in the UHP and LHP by construction. We now consider the large- $|k|$ behaviour of (2.33). The large- $|k|$ behaviour of $F_+(k)$ and $P_-(k)$ is found by considering the behaviour of the unsteady field near the leading edge, which has the typical leading-edge behaviour $\psi \propto \rho^{1/2} \cos(\varphi/2)$ as $\rho \rightarrow 0$. (Here (ρ, φ) are plane polar coordinates in the (x, r) -plane with origin at the splitter leading edge.) From this, it follows that $F_+(k)$ and $P_-(k)$ are both $O(k^{-1/2})$ as $k \rightarrow \infty$ in the corresponding half-plane. The quantities $R_-(k)$ and $L_+(k)$ can be evaluated immediately using (2.30) and (2.31), and are both $O(k^{-1})$ as $k \rightarrow \infty$ in the corresponding half-plane. Finally, the behaviour of the split functions $K_\pm(k)$ is given in Appendix A. Putting all this together, we see that the function defined throughout \mathbb{C} by the respective sides of equation (2.33) is entire and

is $O(1/k)$ for large $|k|$, and so is identically zero by Liouville's Theorem. Hence, we can determine the previously unknown $F_+(k)$ and $P_-(k)$, and hence $A(k)$, and we can invert the Fourier transforms to find the scattered field. The inversion contour lies along the strip of overlap, and we close the contours in the UHP/LHP to obtain the scattered field in $x > 0$, $x < 0$ respectively.

The inversion integrals can be evaluated by the method of residues in the standard way, with the additional complication that the non-isolated singularity at $k = k_c$ is encircled when $x > 0$ and the contour is closed in the UHP. Using the results of the multiple-scales analysis (§2.2 above) the integrand close to $k = k_c$ can be inspected, for instance we find

$$Q_h(r, k) \sim \frac{\sin\left(\frac{2k_c\Omega(r-h)}{U(k-k_c)} + \psi_1\right)}{2\Omega\sqrt{k_c^2 + m^2/s^2}\sin\left(\frac{2k_c\Omega(s-h)}{U(k-k_c)} + \psi_2\right)} \quad \text{as } k \rightarrow k_c \quad (2.34)$$

for certain complicated phases ψ_1, ψ_2 , and the contribution to the integral, if any, from the neighbourhood of $k = k_c$ can be determined. Considering small semi-circular contours above and below k_c it can easily be shown that a non-zero contribution to the potential from $k = k_c$ is only present when $r = s$ in regions I and II. This term is included in the formulae below for completeness, but recalling from §2.2 that for this rigid-body swirling flow any exactly convected mode present in the unsteady potential has zero unsteady velocity and pressure, it has no physical significance. For more general flows analogous exactly convected terms would affect the physical variables, see §3 for more discussion of the significance of these convected terms in other cases. We stress that the potential $\psi(x, r)$ is nevertheless continuous in regions I and II and this is discussed in §2.4 below, alongside the discussion of the convergence of the various infinite sums.

In region I, $x > 0$, $h < r < s$ we find the scattered field

$$\begin{aligned} \psi(x, r) = & -R + \sum_{\nu \in S_{\nu}^+ \cup S_c} e^{i\alpha_{\nu}^+ x} \text{Res}(K)|_{\alpha_{\nu}^+} \left(\frac{\Lambda^2 - 4\Omega^2}{\Lambda K_+} \right)_{\alpha_{\nu}^+} \frac{U_{1\nu}^{(+)}(r)}{U_{1\nu}^{(+)}(s)} \\ & \times \sum_{\mu} \left\{ \frac{B_{1\mu} U_{1\mu}^{(-)}(s)}{(\alpha_{1\nu}^+ - \alpha_{1\mu}^-)} \left(\frac{\Lambda}{(\Lambda^2 - 4\Omega^2)K_-} \right)_{\alpha_{1\mu}^-} - \frac{B_{2\mu} U_{2\mu}^{(-)}(s)}{(\alpha_{1\nu}^+ - \alpha_{2\mu}^-)} \left(\frac{\Lambda}{(\Lambda^2 - 4\Omega^2)K_-} \right)_{\alpha_{2\mu}^-} \right. \\ & \left. + \frac{B_{3\mu}}{\alpha_{1\nu}^+ - \alpha_{3\mu}^+} \left(\frac{\Lambda DK_+}{\Lambda^2 - 4\Omega^2} \right)_{\alpha_{3\mu}^+} \right\} + \frac{\mathcal{A}(r)e^{ik_c x} 2\Omega sm}{U K_+(k_c)(m^2 + k_c^2 s^2/m^2)}, \end{aligned} \quad (2.35)$$

where Res stands for the residue of a function at a pole in the complex plane and $\mathcal{A}(r) = 0$ for $r \neq s$, but

$$\begin{aligned} \mathcal{A}(s) = & \sum_{\mu} \left\{ \frac{B_{1\mu} U_{1\mu}^{(-)}(s)}{(k_c - \alpha_{1\mu}^-)} \left(\frac{\Lambda}{(\Lambda^2 - 4\Omega^2)K_-} \right)_{\alpha_{1\mu}^-} \right. \\ & \left. - \frac{B_{2\mu} U_{2\mu}^{(-)}(s)}{(k_c - \alpha_{2\mu}^-)} \left(\frac{\Lambda}{(\Lambda^2 - 4\Omega^2)K_-} \right)_{\alpha_{2\mu}^-} + \frac{B_{3\mu}}{k_c - \alpha_{3\mu}^+} \left(\frac{\Lambda DK_+}{\Lambda^2 - 4\Omega^2} \right)_{\alpha_{3\mu}^+} \right\}. \end{aligned} \quad (2.36)$$

In Region II, $x > 0$, $s < r < 1$ we find

$$\begin{aligned} \psi(x, r) = & -R + \sum_{v \in S_u^+ \cup S_c} -e^{i\alpha_{2v}^+ x} \text{Res}(K) \Big|_{\alpha_{2v}^+} \left(\frac{\Lambda^2 - 4\Omega^2}{\Lambda K_+} \right)_{\alpha_{2v}^+} \frac{U_{2v}^{(+)}(r)}{U_{2v}^{(+)}(s)} \\ & \times \sum_{\mu} \left\{ \frac{B_{1\mu} U_{1\mu}^{(-)}(s)}{(\alpha_{2v}^+ - \alpha_{1\mu}^-)} \left(\frac{\Lambda}{(\Lambda^2 - 4\Omega^2) K_-} \right)_{\alpha_{1\mu}^-} - \frac{B_{2\mu} U_{2\mu}^{(-)}(s)}{(\alpha_{2v}^+ - \alpha_{2\mu}^-)} \left(\frac{\Lambda}{(\Lambda^2 - 4\Omega^2) K_-} \right)_{\alpha_{2\mu}^-} \right. \\ & \left. + \frac{B_{3\mu}}{\alpha_{2v}^+ - \alpha_{3\mu}^+} \left(\frac{\Lambda D K_+}{\Lambda^2 - 4\Omega^2} \right)_{\alpha_{3\mu}^+} \right\} + \frac{\mathcal{A}(r) e^{ik_c x} 2\Omega s m}{U K_+(k_c) (m^2 + k_c^2 s^2 / m^2)}. \end{aligned} \quad (2.37)$$

And in region III, $x < 0$, $h < r < 1$ we find

$$\begin{aligned} \psi(x, r) = & -L + \sum_{v \in S_u^-} e^{i\alpha_{3v}^- x} \text{Res} \left(\frac{1}{K} \right) \Big|_{\alpha_{3v}^-} \left(\frac{(\Lambda^2 - 4\Omega^2) K_-}{\Lambda} \right)_{\alpha_{3v}^-} \frac{U_{3v}^{(-)}(r)}{D(\alpha_{3v}^-)} \\ & \times \sum_{\mu} \left\{ \frac{B_{1\mu} U_{1\mu}^{(-)}(s)}{(\alpha_{3v}^- - \alpha_{1\mu}^-)} \left(\frac{\Lambda}{(\Lambda^2 - 4\Omega^2) K_-} \right)_{\alpha_{1\mu}^-} \right. \\ & \left. - \frac{B_{2\mu} U_{2\mu}^{(-)}(s)}{(\alpha_{3v}^- - \alpha_{2\mu}^-)} \left(\frac{\Lambda}{(\Lambda^2 - 4\Omega^2) K_-} \right)_{\alpha_{2\mu}^-} + \frac{B_{3\mu}}{\alpha_{3v}^- - \alpha_{3\mu}^+} \left(\frac{\Lambda D K_+}{\Lambda^2 - 4\Omega^2} \right)_{\alpha_{3\mu}^+} \right\}. \end{aligned} \quad (2.38)$$

In these equations the inner sums, over μ , simply cover all the modes present in the incident field, as defined by (2.30) and (2.31). The scattered field contains components at all modes present in the relevant part of the spectrum, including all the (cut-on and cut-off) sonic modes and, in regions I and II, all the nearly-convected modes. The precise amplitude with which a given incident mode is scattered into a given outgoing mode displays complicated dependence on all parameters through the various residue terms and Wiener–Hopf factors, but one broad point can be made. The scattering of a given mode into modes of a similar wavenumber is enhanced, in preference to scattering into modes of disparate wavenumber, by the appearance of factors of the form, for instance $(\alpha_{1v}^+ - \alpha_{1\mu}^-)^{-1}$. Given the relative separation between the families of sonic and nearly-convected wavenumbers evident in figure 2(a), this effect tends to enhance the scattering of a mode from a given family into modes within that family propagating in the same direction (e.g. downstream sonic into downstream sonic).

2.4. Numerical results

We present computations which apply the work of the previous subsection for illustrative parameter values (see caption of figure 3). In particular, the mean flow has a significant swirl component, and we take modest frequency and azimuthal order so that we are not in the high- ω /high- m regime to be considered in §4. For these parameter values there are 2, 2 and 4 cut-on sonic modes in regions I, II and III respectively, and 1, 2 and 2 of them respectively travel downstream. Figure 2 shows the spectrum in region III. Having obtained the axial wavenumbers we can calculate the Wiener–Hopf kernel $K(k)$, which is then factorized using the integration formula (A 1), and hence we can then calculate (2.35)–(2.38). In practice, the infinite tails of the sums in equations (2.35)–(2.38) must be treated with care. Truncation of the sums at (suitably) large $|k|$ is permissible because the large- $|k|$ cut-off sonic modes give an

infinite tail of the form

$$\sum_n n^{-1/2} e^{-n\lambda x} \exp \left\{ i n \int_s^r \sqrt{1 - U^2/c_0^2} dr' \right\} \quad (2.39)$$

for the unsteady pressure in region I (as an example). In (2.39) λ is real and positive and can be found by evaluating (2.15) with the appropriate limits, $(\sigma, t) = (h, s)$. The sum (2.39) is absolutely convergent when $x > 0$. When $x = 0$ it is conditionally convergent (see Hardy 1963, Theorem 196), and converges everywhere except at the leading edge of the splitter plate, $(x, r) = (0, s)$, where the expansion of the unsteady pressure diverges because of the square-root pressure singularity there. However, more care is needed for the infinite series of nearly-convected modes near to $k = k_c$. Consider for instance the field in region I: the asymptotic expressions for the wavenumbers and mode shapes are already known as $k \rightarrow k_c$ (i.e. as $n \rightarrow \pm\infty$ in (2.11) and (2.13)). These results can be used to show that, if α is the wavenumber given by (2.11) with $t = s$ and $\sigma = h$, then

$$\text{Res}(K)|_\alpha \sim \frac{s - h}{U(n\pi)^2 (1 + m^2/(s^2 k_c^2))}. \quad (2.40)$$

Further, since $K_+(k)$ is by definition holomorphic in the UHP one simply gets the leading-order behaviour $K_+(\alpha) \sim K_+(k_c)$ and $\Lambda(\alpha) \sim 2\Omega k_c (s - h)/(n\pi)$ as $\alpha \rightarrow k_c$. Similar results are available in regions II and III. Hence, the infinite sum of the contributions from the nearly-convected modes converges (absolutely) like $\sum 1/n^2$ in the expansion of the pressure. Contributions from the very large- n nearly-convected modes are therefore seen to be small, and of course the exactly convected ($k = k_c$) terms in (2.35)–(2.37) do not contribute to the pressure. In the expansion of the unsteady potential given above the convergence is more delicate however and, considering region I, for $r \neq s$ the nearly convected modes sum like $\sum n^{-1} e^{in\pi(r-s)/(s-h)}$, a sum which is conditionally convergent. When $r = s$ the character of the convergence changes, and cancellation between modes n and $-n$ occurs to ensure convergence which is now of the form $\sum n^{-1} \sin(2\Omega x k_c (s - h)/U n \pi)$. At first sight (2.35), (2.37) appear discontinuous as $r \rightarrow s \pm$ respectively. However, since we can deduce that the potential is continuous as $r \rightarrow s -$ in region I (from the continuity in r of the inversion integral before the contour is deformed near to the singularity at $k = k_c$), we therefore deduce that the discontinuous exactly convected term in (2.35) cancels the discontinuity in the delicate nearly-convected infinite sum, and similarly in (2.37) for $r \rightarrow s +$. We stress again that the exactly convected mode in the unsteady potential has zero unsteady velocity and pressure in this flow, and therefore affects none of the physical variables.

In what follows, computations have been performed by including in the scattered field 40 nearly-convected modes on either side of k_c , and it has been verified that the highest of the included nearly-convected modes are well into the asymptotic regime, with the wavenumbers and residues all agreeing well with the multiple-scales predictions given in §2.1. From all this we can therefore conclude that not only is the scattered field, being made up of an infinite series of contributions, well-defined but also that the finite truncations we have chosen give an accurate solution.

Figure 3 shows the results for a single incident cut-on sonic mode. In figure 3(a) the incident mode is from downstream infinity in region I, which could correspond to noise emanating from an aeroengine core. In this case we see that almost all the disturbance propagates into region III, and that there is very little scattering back

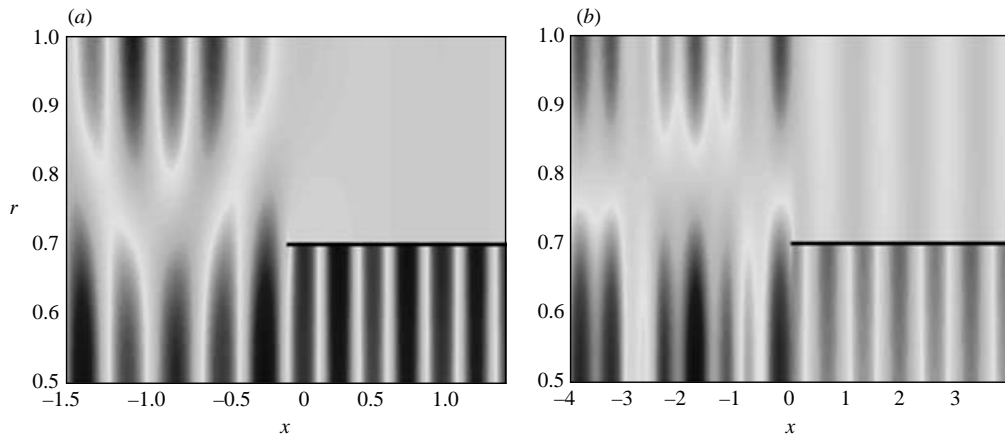


FIGURE 3. The amplitude of the total (incident plus scattered) unsteady pressure due to a single cut-on sonic mode incident from (a) region I, i.e. $x > 0$, $0.5 < r < 0.7$, and (b) region III, i.e. $x < 0$. We have inner duct wall $h = 0.5$ and splitter radius $s = 0.7$, the axial and swirl mean flows are given by $U = \Omega = 0.4$, the frequency is $\omega = 10$ and the azimuthal mode number is $m = 3$. The darkest colours refer to the highest amplitudes. In (a) the incident mode is the only upstream-going cut-on mode in region I, while in (b) the incident mode is the more cut-on of the two downstream-going cut-on modes.

downstream into either regions I or II. In figure 3(b) the incident mode is from upstream infinity in region III, corresponding to downstream-propagating radiation generated by the fan, and we see in this case that the scattered field happens to be stronger in region I than in region II. In figure 3(b) the modulation of the incident field demonstrates that noise is reflected back upstream into region III. We find in these calculations that for incident sonic modes the scattered pressure field is strongly dominated by contributions from the scattered sonic field. However, nearly-convected disturbances are generated at the leading edge (see that in equations (2.35) and (2.37) the scattered modes include the nearly-convected spectrum S_c), and make a significant contribution to the unsteady velocity field. This is in contrast to the case of irrotational mean flow, in which no vortical disturbance is generated at the leading edge and the scattered field is purely irrotational.

If the incident mode is one of the nearly-convected type from upstream (i.e. from region III) we find that both acoustic and nearly-convected scattered modes can contribute to the pressure. For example, we take the incident mode to be the $n = 15$ nearly-convected mode (for which $k = 21.53$, compared to $k_c = 22$), quite far down the tail so that the nearby nearly-convected modes are densely clustered. With this choice we would expect that there are likely to be nearly-convected modes of very similar wavenumber excited in regions I and II, and in fact we do see a noticeable contribution to the downstream scattered pressure from the nearly-convected modes in this case. Figure 4(a) shows the total unsteady pressure at $x = \pm 0$ as a function of r : the agreement of the two provides a check on the correctness of the truncation of the infinite sums and the numerical routines used. The continuity of the pressure across $x = 0$ in this, and all the other cases we have computed, is very good except in the immediate vicinity of the pressure singularity, where of course the infinite sums converge more and more slowly. The close proximity of this singularity is indicated by the larger values taken by the unsteady pressure at $x = 0+$ close to the splitter radius $r = 0.7$. Figure 4(b) shows the unsteady pressure further downstream, at $x = 0.5$. We

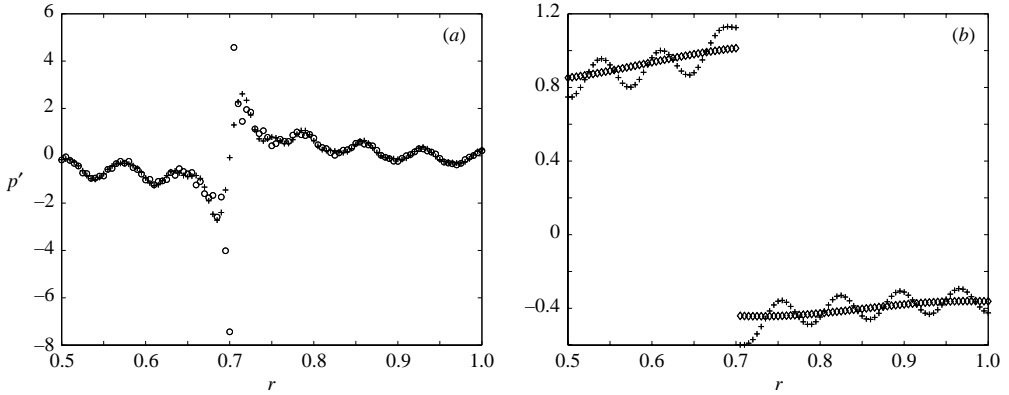


FIGURE 4. The total unsteady pressure due to a single nearly-convected mode ($n = 15$) incident from region III, against r . In (a) the + and \circ symbols refer to the pressure at $x = -0$ (just upstream of the leading edge) and at $x = +0$ (just downstream of the leading edge) respectively. In (b) $x = 0.5$, the + symbols are the total unsteady pressure and the \diamond symbols represent that component of the total unsteady pressure associated with the scattered sonic modes.

see that the unsteady pressure due to the acoustic modes accounts for most of the total unsteady pressure here, but that the nearly-convected modes are contributing noticeably to the total (typically by of the order of 10% in $r \leq 0.7$, but rising to as much as 50% of the total for $r \geq 0.7$).

The contributions from the nearly-convected modes to the scattered pressure which are noticeable in figure 4(b) contrast sharply with the behaviour in the absence of mean vorticity, and also (as we shall see in §4) with the behaviour in the high-frequency regime with swirl. If the mean flow is irrotational *all* the unsteady pressure comes from the acoustic modes, because the vorticity modes carry no pressure at all, while for rotational flow and with ω, m large most of the pressure comes from the acoustic modes. Even in the present $O(1)$ frequency regime, however, if the incident mode is *very* close to pure convection, i.e. in (2.11) $|n| \gg 1$, then almost all of the scattered pressure comes from the sonic modes. nearly-convected modes close to the incident wavenumber will still be excited, but now these are also close to pure convection and so carry little pressure. Consider the incident nearly-convected mode with index n_μ in region III (with $|n_\mu| \gg 1$), for which it follows from (2.35) and (2.11) that the pressure amplitude of the scattered nearly-convected mode with index $n_\nu \gg 1$ in region I, say, is proportional to

$$\frac{1}{n_\nu [(s-h)n_\mu - (1-h)n_\nu]}. \quad (2.41)$$

Quantity (2.41) is typically small for large $n_{\mu,\nu}$, confirming that little pressure will be carried by modes very close to pure convection, but takes its largest value when $n_\nu \approx (s-h)n_\mu / (1-h)$, corresponding to the scattered mode in region I whose wavelength most closely matches that of the incident mode in region III.

3. The trailing-edge problem in rigid-body swirl

We now consider the scattering problem for disturbances interacting with the trailing edge of a splitter plate. For definiteness the geometry we consider is exactly that of figure 1, but now reflected in $x = 0$, and with the axial mean flow still from

left to right. The boundary conditions are still zero radial velocity on the splitter plane, which has now become $x < 0, r = s$. However, now we must also impose the trailing-edge unsteady Kutta condition (Crighton 1985)

$$\lim_{x \rightarrow 0^-} [p'(x, r)]_{r=s^-}^{r=s^+} = 0. \quad (3.1)$$

Within the fluid the pressure is again continuous everywhere, as is the radial velocity, but we allow, as is usual when applying the Kutta condition, for the possibility of a wake sheet to be shed from the trailing edge across which the axial and/or azimuthal velocity may be discontinuous.

The algebraic manipulations of the Wiener–Hopf calculation are similar to those for the leading-edge problem in §2, and are not included in full here. Instead, we highlight briefly the principal differences between the analyses and present the final results.

With the altered geometry described above, the \pm superscripts must be interchanged between (2.30) and (2.31) in order to correctly describe a general incident field. The details of the Wiener–Hopf procedure differ a little, because the half-range transform of the pressure jump on the splitter (denoted $P_-(k)$ in §2) is now a plus-function, and since the zero k_c of $\Lambda(k)$ is in the UHP we cannot divide through by $\Lambda(k)$ to find the Wiener–Hopf equation. Also, the singularity at the trailing edge is weaker than at the leading edge, now of the form $\psi_{tot} \sim \rho^{3/2} \sin(3\varphi/2)$ as $\rho \rightarrow 0$. However, once these points have been noted the analysis can proceed as in §2. Inverting the resulting Fourier transform, we obtain in region I, $x < 0, h < r < s$,

$$\begin{aligned} \psi(x, r) = -L + \sum_{v \in S_a^-} \frac{e^{i\alpha_{1v}^- x} \text{Res}(K)|_{\alpha_{1v}^-}}{(K_- \Lambda)_{\alpha_{1v}^-}} \frac{U_{1v}^{(-)}(r)}{U_{1v}^{(-)}(s)} \sum_{\mu} \left\{ \frac{B_{1\mu} U_{1\mu}^{(+)}(s)}{\alpha_{1v}^- - \alpha_{1\mu}^+} \left(\frac{\Lambda}{K_+} \right)_{\alpha_{1\mu}^+} \right. \\ \left. - \frac{B_{2\mu} U_{2\mu}^{(+)}(s)}{\alpha_{1v}^- - \alpha_{2\mu}^+} \left(\frac{\Lambda}{K_+} \right)_{\alpha_{2\mu}^+} + \frac{B_{3\mu}}{\alpha_{1v}^- - \alpha_{3\mu}^-} (D \Lambda K_-)_{\alpha_{3\mu}^-} \right\}; \quad (3.2) \end{aligned}$$

in region II, $x < 0, s < r < 1$,

$$\begin{aligned} \psi(x, r) = -L + \sum_{v \in S_a^-} -\frac{e^{i\alpha_{2v}^- x} \text{Res}(K)|_{\alpha_{2v}^-}}{(K_- \Lambda)_{\alpha_{2v}^-}} \frac{U_{2v}^{(-)}(r)}{U_{2v}^{(-)}(s)} \sum_{\mu} \left\{ \frac{B_{1\mu} U_{1\mu}^{(+)}(s)}{\alpha_{2v}^- - \alpha_{1\mu}^+} \left(\frac{\Lambda}{K_+} \right)_{\alpha_{1\mu}^+} \right. \\ \left. - \frac{B_{2\mu} U_{2\mu}^{(+)}(s)}{\alpha_{2v}^- - \alpha_{2\mu}^+} \left(\frac{\Lambda}{K_+} \right)_{\alpha_{2\mu}^+} + \frac{B_{3\mu}}{\alpha_{2v}^- - \alpha_{3\mu}^-} (D \Lambda K_-)_{\alpha_{3\mu}^-} \right\}; \quad (3.3) \end{aligned}$$

and in region III, $x > 0, h < r < 1$,

$$\begin{aligned} \psi(x, r) = -R + \sum_{v \in S_a^+ \cup S_c} e^{i\alpha_{3v}^+ x} \text{Res} \left(\frac{1}{K} \right) \Big|_{\alpha_{3v}^+} \left(\frac{K_+}{\Lambda D} \right)_{\alpha_{3v}^+} U_{3v}^{(+)}(r) \\ \times \sum_{\mu} \left\{ \frac{B_{1\mu} U_{1\mu}^{(+)}(s)}{\alpha_{3v}^+ - \alpha_{1\mu}^+} \left(\frac{\Lambda}{K_+} \right)_{\alpha_{1\mu}^+} - \frac{B_{2\mu} U_{2\mu}^{(+)}(s)}{\alpha_{3v}^+ - \alpha_{2\mu}^+} \left(\frac{\Lambda}{K_+} \right)_{\alpha_{2\mu}^+} + \frac{B_{3\mu} (D \Lambda K_-)_{\alpha_{3\mu}^-}}{\alpha_{3v}^+ - \alpha_{3\mu}^-} \right\} \\ + \frac{\mathcal{B}(r) e^{ik_c x} K_+(k_c)}{2U}. \quad (3.4) \end{aligned}$$

The final term in (3.4) corresponds to a contribution to the unsteady potential from the non-isolated singularity at $k = k_c$, with $\mathcal{B}(r) = 0$ for $r \neq s$ but

$$\mathcal{B}(s\pm) = \pm \sum_{\mu} \left\{ \frac{B_{1\mu} U_{1\mu}^{(+)}(s)}{k_c - \alpha_{1\mu}^{+}} \left(\frac{\Lambda}{K_+} \right)_{\alpha_{1\mu}^{+}} - \frac{B_{2\mu} U_{2\mu}^{(+)}(s)}{k_c - \alpha_{2\mu}^{+}} \left(\frac{\Lambda}{K_+} \right)_{\alpha_{2\mu}^{+}} + \frac{B_{3\mu} (D \Lambda K_-)_{\alpha_{3\mu}^{-}}}{k_c - \alpha_{3\mu}^{-}} \right\}. \quad (3.5)$$

Exactly as in the leading edge case in §2.3, the exactly convected term in (3.4) ensures that the potential $\psi(x, r)$ is continuous as $r \rightarrow s-$ from below, and as $r \rightarrow s+$ from above, and arises because of the delicate conditional convergence of the infinite sum of contributions of nearly-convected modes. We see that the potential, although continuous as r approaches s from above or below, is discontinuous across $r = s$, the discontinuity being given by twice the exactly convected term in (3.4). However, the unsteady pressure and the total unsteady velocity are continuous across $r = s$. The fact that the unsteady pressure is continuous follows simply from the fact that the $k = k_c$ mode has zero associated pressure. The continuity of all three components of unsteady velocity depends on the fact that we are here considering rigid-body swirl with uniform axial mean flow, and as argued in §2.2 the total unsteady velocity associated with the $k = k_c$ mode is zero. This behaviour is in contrast to the case of general swirl and axial mean flow distributions, for which a wake sheet would generally be present on $r = s$, across which the axial and azimuthal components of the total velocity would jump as a result of a discontinuous potential. In §4.4, where we consider more general mean flows, such a wake sheet is indeed present.

It is interesting to note that for uniform axial mean flow, although a wake sheet is absent for any $\Omega \neq 0$ (as argued in the previous paragraph), one is present when $\Omega = 0$. In fact, the calculation in §2.2 that the $k = k_c$ mode has zero total velocity fails when $\Omega = 0$, and ultimately the difference in behaviour between the $\Omega = 0$ and $\Omega \neq 0$ cases can be tracked down to the presence of the factor

$$\frac{\Lambda^2}{\Lambda^2 - 4\Omega^2} \quad (3.6)$$

multiplying the highest derivative in (2.7) (as well as appearing in relations such as (2.10)). The factor (3.6) reduces to zero as $k = k_c$ is approached (recall from (2.9) that $\Lambda \propto k - k_c$) for any $\Omega \neq 0$, but when $\Omega = 0$ the factor (3.6) is unity. This is the reason why the wake sheet, having been absent in the calculation of the present section with $\Omega \neq 0$, then appears when $\Omega = 0$, as described by Rienstra (1984) and Howe (1986) who both studied problems in uniform mean flow with no swirl.

A further note to make about the results presented for this scattering problem is that the results of Rienstra (1984) for a similar problem in uniform mean flow can be recovered in the limit $\Omega \rightarrow 0$, and we shall outline the correspondence here. Letting $\Omega \rightarrow 0$ the mode-shape equation (2.7) becomes Bessel's equation and the quantities $Q_i(r, k)$, $Q_h(r, k)$ and $K(k)$ defined above can be written explicitly in terms of Bessel and Hankel functions. Setting the outer radius of the duct to infinity recovers Rienstra's geometry. After a little manipulation the kernel $K(k)$ can be expressed in terms of the kernel defined in Rienstra (1984), which we denote by K^R , and (noting the different Fourier transform convention used) we can therefore identify

$$\frac{1}{\Lambda K_-} \equiv \frac{w_+^2 k K_+^R}{\sqrt{2}}, \quad \frac{1}{K_+} \equiv \frac{w_-^2 k K_-^R}{\sqrt{2}}, \quad (3.7)$$

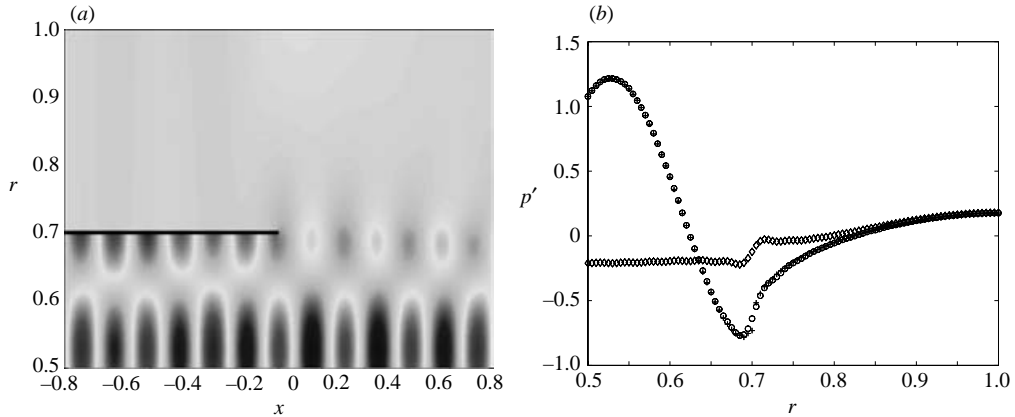


FIGURE 5. (a) The total unsteady pressure, for a single nearly-convected mode incident on the trailing edge from region I, other conditions as in figure 3. In (b) the total unsteady pressure at $x = \pm 0$ is denoted with $+$ and \circ symbols respectively, while the unsteady pressure at $x = +0$ associated purely with the scattered sonic modes is denoted with \diamond symbols.

where the w_{\pm} are defined in Rienstra (1984). It is then straightforward to verify that the inversion integral in Rienstra (1984), for which the full Kutta condition is enforced ($\gamma = 1$ in the notation of that paper), is recovered by the $\Omega = 0$ case of our solution to the present problem. Indeed, one can verify by inspection of the inversion integral before it is evaluated by the method of residues that the pressure jump across $r = s$ is zero for $x > 0$ and behaves like $A|x|^{1/2}$ as $x \rightarrow 0^-$, and that the full Kutta condition (3.1) is satisfied by (3.2)–(3.4) when $\Omega \neq 0$ as well, as required.

We now present results for the same parameter values as in the leading-edge case. For the trailing edge, sonic modes again predominantly scatter into sonic modes. The mechanism for noise generation at the trailing edge is provided by the fact that the wake cannot support a pressure jump, so that a scattered field is produced to cancel the pressure jump present in the incident field. The Kutta condition (3.1) then implies that the scattered pressure will be of the same order of magnitude as the pressure associated with the incident mode. For an incident mode of the nearly-convected type, this heuristic argument suggests that the pressure in the scattered acoustic field will never dominate over the pressure fields associated with the incident and scattered nearly-convected contributions. We find in our computations that the nearly-convected modes always contribute significantly to the scattered pressure (this is also seen at high frequency in §4), and that the picture is qualitatively the same for all nearly-convected modes. Figure 5(a) shows the unsteady pressure field for a nearly-convected mode incident from region I, while figure 5(b) shows the total unsteady pressure distribution across the duct just upstream and just downstream of the trailing edge. Note that the agreement between $+$ and \circ symbols confirms the continuity of our solutions (3.2)–(3.4), and that there is no pressure singularity at the trailing edge (as stipulated in equation (3.1)). Significantly, the contribution to the total scattered pressure from the scattered sonic disturbances is quite a small fraction of the total pressure inboard of the line of the splitter, where the incident and scattered nearly-convected disturbances dominate (recall that the incident nearly-convected disturbance originates in $r \leq 0.7$). As one would expect, only a very small nearly-convected field is induced in $x > 0$ outboard of the splitter, where the scattered sonic field is consequently dominant. This is all in contrast to what would happen in

the absence of mean vorticity, in which case the convected disturbance would convect past the trailing edge with zero pressure, and *no* scattered pressure field would be produced.

4. Scattering in the limit of large azimuthal order

In this section we will suppose that the azimuthal order, m , is large. This follows the asymptotic approach used in Cooper & Peake (2005), who studied the propagation of nearly-convected and sonic disturbances along an infinite duct in swirling flow. In the aeroengine context, unsteady flow generated by the rotor has tonal components with frequencies which are integer multiples of $B\Omega_F$, where B is the number of fan blades and Ω_F is the fan rotation rate, and azimuthal orders, m , which are integer multiples of B . The blade number is often large (between 20 and 30), so that the limit $m \gg 1$ with $\omega = O(m)$ is a practically relevant limit. The great advantage of making the large- m approximation is that the resulting simplification will allow us to study a much wider class of mean flows than the rigid-body swirl case of the previous two sections.

4.1. The infinite duct

In this subsection we present results from Cooper & Peake (2005) for an infinite duct, which will be required in our scattering problem. The governing equations are (2.4) and (2.5) as before, but the mean flow now takes the more general form

$$\mathbf{U}_0(r) = U_x(r)\mathbf{e}_x + U_\theta(r)\mathbf{e}_\theta. \quad (4.1)$$

It turns out that the sonic and nearly-convected parts of the spectrum are described by different scalings with m . For the sonic part of the spectrum, we write the unsteady velocity and potential as

$$\mathbf{u} = A(r)e^{ikx+im\theta-i\omega t}, \quad \phi = \Phi(r)e^{ikx+im\theta-i\omega t}. \quad (4.2)$$

The axial wavenumber is supposed large, with the preferred scaling $k = O(m)$, and since these modes are pressure-dominated with most of their velocity coming from the irrotational part of the unsteady velocity we choose $|\mathbf{u}| = O(\phi)$. This scaling leads to an entirely consistent expansion in powers of $1/m$ (or $1/B$), see Cooper & Peake (2005). To leading order in m , equation (2.5) then reduces to the second-order ODE

$$\frac{d^2\Phi}{dr^2} = -m^2 f \Phi \quad \text{where} \quad f(r) \equiv \frac{(U_\theta/r - \omega/m + U_x k/m)^2}{c_0^2} - \frac{1}{r^2} - \frac{k^2}{m^2}, \quad (4.3)$$

with boundary condition $d\Phi/dr = 0$ at the outer and inner duct radii. This yields an eigenvalue problem for k , which is solved using the WKB method as described in §5.1 of Cooper & Peake (2005). In fact, when k is real (4.3) can have one or more turning points, where $f(r) = 0$. A turning point corresponds physically to a *caustic* cylinder, as described by Chapman (1994). A uniformly-valid composite expression for the eigenfunctions is not given in Cooper & Peake (2005), but will be required for our subsequent analysis (Cooper & Peake 2005 simply present the inner Airy function and outer (singular) WKB solutions.) We therefore employ Langer's solution (details in Bender & Orszag 1978) to (4.3), which gives an approximation which is uniformly valid in r as $m \rightarrow \infty$. If $r = c$ is the turning point, then the Langer solution is of the form

$$\left. \begin{aligned} \Phi &= S_0^{1/6}(r)(f(r))^{-1/4} \left[\alpha \text{Ai}((3|m|S_0(r)/2)^{2/3}) + \beta \text{Bi}((3|m|S_0(r)/2)^{2/3}) \right], \\ S_0(r) &\equiv \int_c^r \sqrt{-f(r')} dr'. \end{aligned} \right\} \quad (4.4)$$

A ratio between the arbitrary constants α, β follows from one boundary condition, and an implicit equation to be solved for the eigenvalue k follows from the second boundary condition (note that c depends on k). Langer's solution (4.4) reduces to the Airy/WKB solutions given in Cooper & Peake (2005) very close to/far from $r = c$, and is found to give better agreement with direct numerical integration. Multiple turning points can also be treated by defining several Langer-type solutions, one for each turning point. These expressions are then 'stitched' together by enforcing continuity of Φ and $d\Phi/dr$, for example midway between consecutive turning points, to give a uniformly valid approximation over the whole interval. (See Bender & Orszag 1978, §10.5.)

Turning now to the nearly-convected part of the spectrum and again closely following Cooper & Peake (2005), we consider the equations governing a high-frequency nearly-convected disturbance. In the large- m limit the entire nearly-convected family of eigenvalues have the same locally convected wavenumber, i.e. $k = k^*(r) = O(m)$ with $\omega - mU_\theta(r)/r - k^*(r)U_x(r) = 0$, but with amplitude depending on position. This leads to

$$\mathbf{u} = \mathbf{A}(x, r)e^{ik^*(r)x + im\theta - i\omega t}, \quad \phi = \Phi(x, r)e^{ik^*(r)x + im\theta - i\omega t}. \quad (4.5)$$

Here we expect the rotational and irrotational parts to contribute equally to the velocity, and therefore take the scaling $|\mathbf{A}| = O(m\Phi)$. The downstream evolution of $\mathbf{A}(x, r)$ is then described by a set of three first-order ODEs of the form

$$\frac{\partial \mathbf{A}}{\partial x} = \mathcal{M}(x, r)\mathbf{A}, \quad (4.6)$$

given in equations (16)–(18) of Cooper & Peake (2005), while the potential Φ is slaved to $\mathbf{A}(x, r)$ and is given by equation (19) of Cooper & Peake (2005). Downstream of some prescribed initial condition (4.6) can be solved analytically, details are given in Appendix B, but it turns out that the boundary conditions at the walls cannot in general be satisfied. In Cooper & Peake (2005) hydrodynamic boundary layers of thickness $O(1/m)$ are introduced at each wall, which define correction terms to ensure that the boundary conditions are satisfied – this is described in §2.2 of Cooper & Peake (2005).

In summary, we have presented the large- m description of unsteady flow in an infinite duct. The total unsteady field is made up of three components: the sonic field given by (4.4); the nearly-convected field in the body of the fluid, given as the solution of (4.6); and the boundary-layer correction localized on the walls to satisfy the boundary conditions. We will now use this description to study scattering problems in the large- m regime.

4.2. Scattering of sonic modes at the leading edge

Here we attempt the large- m solution of the scattering of incident sonic modes by the leading edge. The solution proceeds almost as in the exact case of §2.3, but with certain key differences which we will mention here. We denote the solution of the WKB equation (4.3) with $\partial\Phi/\partial r = 0, 1$ at $r = h, s$ respectively as $Q_h(r, k)$, and the solution with $\partial\Phi/\partial r = 0, 1$ at $r = 1, s$ is denoted $Q_i(r, k)$. Note that these $Q_{i,h}$ are slightly different from those in §2.3. Then using the fact that $\partial\phi/\partial r$ is continuous everywhere, we write for the full-range Fourier transform of the unsteady velocity potential

$$\hat{\psi}(r, k) = \begin{cases} A(k)Q_h(r, k), & h < r < s \\ A(k)Q_i(r, k), & s < r < 1, \end{cases} \quad (4.7)$$

with $A(k)$ at this stage unknown. A Wiener–Hopf analysis proceeds as before with kernel, denoted $K^h(k)$, given by (2.29) (but with $Q_{h,t}$ as given in this subsection). The asymptotic behaviour of $K^h(k)$ for $k \rightarrow \infty$ is different to what is given in Appendix A for $K(k)$. Now we have $K^h(k) \sim 1/(\mathcal{C}|k|)$ as $k \rightarrow \infty$ with $\mathcal{C} = -\frac{1}{2}\sqrt{1 - U_x^2(s)/c_0^2(s)}$, and $K_{\pm}^h(k) = O(k^{-1/2})$ as $k \rightarrow \infty$ in the appropriate half-plane. Otherwise, the procedure in Appendix A for decomposing $K(k)$ can be applied to $K^h(k)$ as well. In particular $K^h(k)$ is also meromorphic, as the continuous spectrum present for a general mean flow has been decoupled from the sonic spectrum by the asymptotic scaling in §4.1, and is again absent from the Wiener–Hopf kernel.

After some straightforward manipulations, we present the final results for the scattered field as follows. In region I, $x > 0, h < r < s$ we have for the unsteady potential

$$\begin{aligned} \psi(x, r) = & -R + \sum_{v=1}^{\infty} \frac{e^{i\alpha_{1v}^+ x} \text{Res}(K^h)|_{\alpha_{1v}^+} U_{1v}^{(+)}(r)}{K_+^h(\alpha_{1v}^+) U_{1v}^{(+)}(s)} \\ & \times \sum_{\mu=1}^{\infty} \left\{ \frac{B_{3\mu} K_+^h(\alpha_{3\mu}^+) U_{3\mu}^{(+)\prime}(s)}{\alpha_{1v}^+ - \alpha_{3\mu}^+} + \frac{B_{1\mu} U_{1\mu}^{(-)}(s)}{(\alpha_{1v}^+ - \alpha_{1\mu}^-) K_-^h(\alpha_{1\mu}^-)} - \frac{B_{2\mu} U_{2\mu}^{(-)}(s)}{(\alpha_{1v}^+ - \alpha_{2\mu}^-) K_-^h(\alpha_{2\mu}^-)} \right\}. \end{aligned} \quad (4.8)$$

In Region II, $x > 0, s < r < 1$, we have

$$\begin{aligned} \psi(x, r) = & -R + \sum_{v=1}^{\infty} - \frac{e^{i\alpha_{2v}^+ x} \text{Res}(K^h)|_{\alpha_{2v}^+} U_{2v}^{(+)}(r)}{K_+^h(\alpha_{2v}^+) U_{2v}^{(+)}(s)} \\ & \times \sum_{\mu=1}^{\infty} \left\{ \frac{B_{3\mu} K_+^h(\alpha_{3\mu}^+) U_{3\mu}^{(+)\prime}(s)}{\alpha_{2v}^+ - \alpha_{3\mu}^+} + \frac{B_{1\mu} U_{1\mu}^{(-)}(s)}{(\alpha_{2v}^+ - \alpha_{1\mu}^-) K_-^h(\alpha_{1\mu}^-)} - \frac{B_{2\mu} U_{2\mu}^{(-)}(s)}{(\alpha_{2v}^+ - \alpha_{2\mu}^-) K_-^h(\alpha_{2\mu}^-)} \right\}. \end{aligned} \quad (4.9)$$

And in region III, $x < 0, h < r < 1$,

$$\begin{aligned} \psi(x, r) = & -L + \sum_{v=1}^{\infty} e^{i\alpha_{3v}^- x} K_-^h(\alpha_{3v}^-) \text{Res}\left(\frac{1}{K^h}\right)\Big|_{\alpha_{3v}^-} \frac{U_{3v}^{(-)}(r)}{U_{3v}^{(-)\prime}(s)} \\ & \times \sum_{\mu=1}^{\infty} \left\{ \frac{B_{3\mu} K_+^h(\alpha_{3\mu}^+) U_{3\mu}^{(+)\prime}(s)}{\alpha_{3v}^- - \alpha_{3\mu}^+} + \frac{B_{1\mu} U_{1\mu}^{(-)}(s)}{(\alpha_{3v}^- - \alpha_{1\mu}^-) K_-^h(\alpha_{1\mu}^-)} - \frac{B_{2\mu} U_{2\mu}^{(-)}(s)}{(\alpha_{3v}^- - \alpha_{2\mu}^-) K_-^h(\alpha_{2\mu}^-)} \right\}. \end{aligned} \quad (4.10)$$

Here $1 \leq v, \mu < \infty$ label the sonic modes, with $v, \mu = 1$ being the most cut-on mode in the corresponding half-plane. Note that equations (4.8)–(4.10) are similar to the $m = O(1)$ analogues (2.35)–(2.38), but there are important differences. In particular, as already noted, the Wiener–Hopf kernel has different behaviour for large $|k|$. Importantly, the formulae of §2.3 include the nearly-convected spectrum for that problem exactly, while here the effect of the nearly-convected spectrum appears at a higher order in $1/m$ and is therefore absent. Recall that (2.35)–(2.38) are restricted to a particular (rigid-body) mean flow, whereas these asymptotic results hold for sonic scattering in a general mean flow. Nevertheless, a large- m limit, with $\omega, k = O(m)$, of equations (2.35)–(2.38) can be taken. First, note that $|A| \rightarrow \infty$ as $|k| \rightarrow \infty$, so that only the high-frequency *sonic* modes are obtained. Further, if we restrict attention in the large- m limit to rigid-body swirl, then it is easy to show that $\Lambda(k)K_-(k) \sim K_-^h(k)$ and $K_+(k) \sim K_+^h(k)$ as $m \rightarrow \infty$, while $|2\Omega/\Lambda(k)| \ll 1$. In this way, equations (4.8)–(4.10) are recovered exactly from the exact equations (2.35)–(2.38). However, we emphasize again that the results presented in this subsection are applicable to much more general mean flows than the rigid-body-swirl results of §2.3, albeit only at large m .

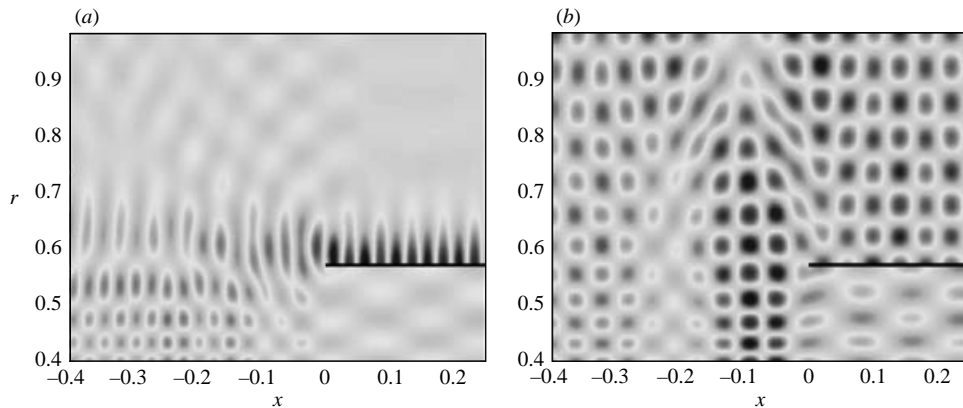


FIGURE 6. Unsteady pressure in the duct for (a) the first ($\mu = 1$) and (b) the eighth ($\mu = 8$) cut-on sonic modes, incident from downstream in region II. Here we take the radii of the hub and splitter as $h = 0.391$ and $s = 0.569$, the azimuthal order is $m = -48$, the frequency is $\omega = 46.8$, the mean axial flow is $U_x(r) = 1/2$ and the mean swirl is $U_\theta = 0.1r + 0.25/r$.

We now present computations using parameter values (see figure 6) mostly originating from Nijboer & Sijtsma (1998) and Cooper & Peake (2005). Note that the general mean flows treated in this section can now include unstable flows, however results are only presented for flows which were found to be stable. For the chosen parameter values there are 9, 16 and 23 cut-on sonic modes in regions I, II and III respectively, of which 4, 8 and 11 are upstream-propagating. Figure 6 shows plots of the pressure for two different incident cut-on sonic modes propagating upstream from region II (in practical terms representing noise from the downstream stator). In figure 6(a) the incident wave mode has a caustic cylinder just outboard of the splitter radius, and is exponentially small outside this caustic cylinder. There is no sufficiently similar mode available in region III for this incident mode to be predominantly scattered into, and instead we see a complete redistribution of energy over several radial modes in region III. The picture is reminiscent of a ring source located at the tip of the splitter, indicating the predominance of the field diffracted from the leading edge. In figure 6(b) the incident wave is of higher radial order, and the caustic has now disappeared from the duct so that the incident mode has significant amplitude over all of region II. We now see noise scattered into all three regions, including back downstream into region I. It is important to note that the presence of the leading edge can have a significant effect on the sonic mode propagating upstream. The incident mode does not simply propagate straight past the edge; diffraction leads to a complicated near field, while in the far field, say $x < -0.3$ in figure 6(b), the field in region III is typically dominated by a disturbance of roughly the same axial wavelength and mode shape (in $r \geq s$ at least) as the incoming disturbance.

The large- m limit of the problem described in §3 of the scattering of sonic modes at a splitter *trailing* edge has also been completed, and the qualitative conclusions are very similar to the leading-edge results above (however note that, having abandoned the specialized mean flow of §3, the usual wake sheet is present downstream of the trailing edge, as expected, just as it is present in §4.4 below). In the next subsection we will therefore consider instead the large- m scattering of nearly-convected disturbances, and here the effects of the mean-flow vorticity will be crucial.

4.3. *Scattering of a nearly-convected mode at a leading edge*

We now consider the scattering of an incident nearly-convected disturbance by the leading-edge geometry of figure 1. Recall from §4.1 that in the large- m limit the nearly-convected disturbance has the form away from the walls of a profile which marches downstream according to an equation of the form (4.6), plus a boundary-layer correction in layers of width $O(1/m)$ near the walls to ensure zero normal velocity on the walls.

For the leading-edge scattering problem we define an inner region around the leading edge of axial and radial extent $O(1/m)$, with inner coordinates $R = |m|(r - s)$, $X = |m|x$. Applying this inner scaling to equation (2.4) and using the decomposition (4.5), we find to leading order

$$\frac{\partial \mathbf{A}}{\partial X} = 0. \quad (4.11)$$

Furthermore, the rescaled equation for the potential has a left-hand side which is simply the rescaled wave operator (i.e. the operator on the left of (2.5) with x and r replaced by X and R), while the source term present on the right-hand side of (2.5) turns out to be at a smaller order in m than the left-hand side, and is therefore neglected.

Now we describe the various terms present in the solution of this scattering problem, as follows:

(a) Away from the splitter the nearly-convected disturbance, and the boundary-layer corrections on the inner and outer duct walls, are simply marched downstream and are unaffected by the presence of the splitter. They will be augmented by additional terms generated at the splitter leading edge.

(b) To satisfy the condition of zero radial velocity on the splitter, a correction must be generated to cancel the upwash on the splitter from the nearly-convected disturbance. This upwash is of the form $v(x)e^{ik^*(s)x}$, where we recall that $k^*(r) = O(m)$ is the convected axial wavenumber at radius r and $v(x)$ is known. To do this we solve a scattering problem in the inner region, leading to a correction term which has upwash $-v(0)e^{ik^*(s)X/|m|}$ on $R=0$, $X > 0$. This correction term must be purely sonic, because from (4.11) the nearly-convected flow does not evolve in the inner region, so that throughout the inner region \mathbf{A} is constant and given by the upstream inner limit of the incident disturbance.

(c) A further correction must be introduced to cancel the remaining upwash on $r = s \pm$, $x > O(1/m)$ in the outer region, i.e. this correction must have upwash

$$-[v(x) - v(0)] e^{ik^*(s)x}, \quad r = s \pm, x > 0. \quad (4.12)$$

Note how term (c) arises from the way in which the sonic field generated at the leading edge, point (b) above, only cancels the incident upwash exactly in the inner region. Correction term (c) is a hydrodynamic disturbance which decays exponentially away from the boundary layers on either side of the splitter plate, and therefore does not contribute significantly to the sound in the duct. Putting all this information together, the problem for determining the sound in the duct has reduced to that of finding the scattered sonic potential in point (b) above, and this is done using exactly the solution method in the previous subsection, but now with the boundary condition $\partial\phi/\partial r = -v(0)e^{ik^*(s)x}$ on $r = s \pm$, $x > 0$. Note that the scattered field will simply be proportional to the incident upwash at the leading edge. Also, the pressure of the scattered sonic field dominates the pressure field of the incident nearly-convected disturbance and of the boundary-layer corrections, both of which possess a convected

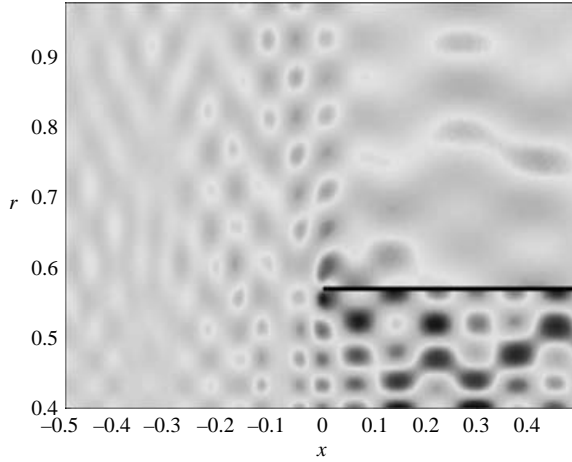


FIGURE 7. The unsteady pressure of the scattered sonic field, with the nearly-convected disturbance incident from upstream infinity. Other conditions as in figure 6.

phase. Having reduced the problem to another Wiener–Hopf problem for the scattered field, we simply state the result for the scattered potential: in region I, $x > 0$, $h < r < s$

$$\psi = -v(0)e^{ik^*(s)x} Q_h(r, k^*(s)) - v(0)K_+^h(k^*(s)) \sum_{\mu=1}^{\infty} \frac{e^{i\alpha_{1\mu}^+ x} \text{Res}(K^h)|_{\alpha_{1\mu}^+}}{K_+^h(\alpha_{1\mu}^+)(k^*(s) - \alpha_{1\mu}^+)} \frac{U_{1\mu}^{(+)}(r)}{U_{1\mu}^{(+)}(s)}; \quad (4.13)$$

in region II, $x > 0$, $s < r < 1$

$$\psi = -v(0)e^{ik^*(s)x} Q_t(r, k^*(s)) + v(0)K_+^h(k^*(s)) \sum_{\mu=1}^{\infty} \frac{e^{i\alpha_{2\mu}^+ x} \text{Res}(K^h)|_{\alpha_{2\mu}^+}}{K_+^h(\alpha_{2\mu}^+)(k^*(s) - \alpha_{2\mu}^+)} \frac{U_{2\mu}^{(+)}(r)}{U_{2\mu}^{(+)}(s)}; \quad (4.14)$$

and in region III, $x < 0$, $h < r < 1$

$$\psi = -v(0)K_+^h(k^*(s)) \sum_{\mu=1}^{\infty} \frac{e^{i\alpha_{3\mu}^- x} K_-^h(\alpha_{3\mu}^-) \text{Res}(1/K^h)|_{\alpha_{3\mu}^-}}{(k^*(s) - \alpha_{3\mu}^-)} \frac{U_{3\mu}^{(-)}(r)}{U_{3\mu}^{(-)}(s)}. \quad (4.15)$$

The first terms in (4.13) and (4.14) provide the upwash to satisfy the splitter boundary condition. They are convected and pressure-less when $r = s$, and are localized near $r = s$. This latter point follows because the wavenumber $k = k^*(s)$ lies well away from the sonic wavenumbers in the axial eigenvalue plane, and a standard WKB analysis can be used to show that $Q_{h,t}(r, k^*(s))$ decay exponentially away from $r = s$. The remaining terms in (4.13)–(4.14) and all the terms in (4.15) are the scattered acoustic field.

The pressure of the scattered acoustic field is plotted in figure 7. The only information from the incident disturbance that is needed to find the scattered field is $v(0)$, the upwash at the splitter leading edge, and since this only acts as a multiplicative constant on the whole field it is set to be unity, so that without any detailed knowledge of a particular incident nearly-convected disturbance we see the generic response. Figure 7 shows that the scattering at the leading edge produces significant noise in all three regions – so that in the aeroengine application noise is propagating downstream toward the engine and into the bypass as well as back upstream toward the fan.

4.4. *Scattering of a nearly-convected mode at a trailing edge*

The final problem to be considered is that of an incident nearly-convected disturbance impinging on a splitter-plate trailing-edge geometry. In contrast to the leading-edge problem in the previous subsection, where the incident gust had a non-zero upwash on the splitter which had to be cancelled by the introduction of a scattered sonic field, in the trailing-edge problem the downstream continuation of the incident disturbance (including the associated wall boundary layer) does not violate the condition of continuous normal velocity across the wake. Instead, we must impose continuity of disturbance pressure in the fluid downstream, together with the unsteady Kutta condition at the trailing edge. Specifically, if we suppose that the incident disturbance is simply marched downstream, with the (incorrect) rigid-wall boundary condition in $x > 0$, then this incident disturbance will possess a pressure jump

$$[p'_{inc}]_{s-}^{s+} = \Delta p(x) e^{ik^*(s)x} \quad (4.16)$$

across $r = s$ for all x . The scattered field from the trailing edge is then introduced to cancel this pressure jump, i.e. the scattered field has a pressure jump

$$[p'_{scat}]_{s-}^{s+} = -\Delta p(x) e^{ik^*(s)x} \quad \text{in } x > 0, \quad (4.17)$$

and such that

$$\lim_{x \rightarrow 0-} [p'_{scat}]_{s-}^{s+} = -\Delta p(0) e^{ik^*(s)x}, \quad (4.18)$$

so that the Kutta condition of zero pressure jump at the trailing edge is satisfied.

Just as was done at the leading edge, we consider an inner region of radial and axial extent $O(1/|m|)$ around the trailing edge. Again, because the nearly-convected quantities necessarily propagate downstream, and only a sonic correction can propagate upstream from the trailing edge, our scattered field must have $A = 0$ in the inner region. So in the same vein as before, the inner problem is a Wiener-Hopf problem for a scattered sonic disturbance, and we find this field by considering the two-part boundary-value problem in the inner region in which the sonic scattered waves have zero radial velocity on the splitter $R = 0$, $X < 0$, with continuous normal (radial) velocity across the wake sheet $R = 0$, $X > 0$, with an imposed pressure jump across $R = 0$ of

$$-\Delta p(0) e^{ik^*(s)x} \quad \text{in } X > 0, \quad (4.19)$$

and such that the scattered pressure jump satisfies the Kutta condition (4.18). Further downstream, away from the inner region, another correction term must be found to cancel the remaining pressure jump of $[\Delta p(x) - \Delta p(0)] e^{ik^*(s)x}$ across the wake sheet.

At this point a significant difference from the leading-edge problem becomes apparent, because the nature of the boundary conditions means that the new correction terms have pressures which are at most of the same order of magnitude as the incident pressure jump across the splitter. This means that the scattered sonic field no longer dominates the total unsteady pressure, which must now be calculated by including contributions from the incident disturbance and the wake sheet, along with the scattered sonic field.

The input to our calculation is provided by considering a nearly-convected disturbance propagating along the duct upstream, exactly as calculated in Cooper & Peake (2005). Figure 8 shows the pressure of the incident disturbance; the boundary-layer structure, in which the largest unsteady pressures are concentrated near the walls, is clearly visible.

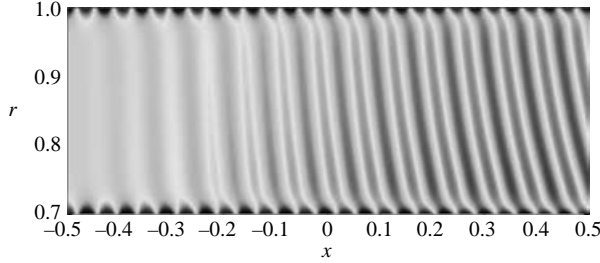


FIGURE 8. The unsteady pressure of an incident disturbance propagating downstream in the duct $0.7 \leq r \leq 1$, with azimuthal order $m = 52$, frequency $\omega = 78$, mean axial flow $U_x(r) = 0.7$ and mean swirl $U_\theta = 0.2r + 0.1/r$.

The first step in our scattering calculation is the sonic problem for the scattered unsteady potential from the inner region at the trailing edge. This Wiener–Hopf problem is again similar to those solved previously, and we find that: in region I, $x < 0, h < r < s$,

$$\psi(x, r) = \frac{-i\Delta p(0)}{\rho_0(s)U_x(s)K_+^h(k^*(s))} \sum_{\nu=1}^{\infty} \frac{e^{i\alpha_{1\nu}^- x} \text{Res}(K^h)|_{\alpha_{1\nu}^-}}{K_-^h(\alpha_{1\nu}^-)(\alpha_{1\nu}^- - k^*(s))^2} \frac{U_{1\nu}^{(-)}(r)}{U_{1\nu}^{(-)}(s)}; \quad (4.20)$$

in region II, $x < 0, s < r < 1$,

$$\psi(x, r) = \frac{i\Delta p(0)}{\rho_0(s)U_x(s)K_+^h(k^*(s))} \sum_{\nu=1}^{\infty} \frac{e^{i\alpha_{2\nu}^- x} \text{Res}(K^h)|_{\alpha_{2\nu}^-}}{K_-^h(\alpha_{2\nu}^-)(\alpha_{2\nu}^- - k^*(s))^2} \frac{U_{2\nu}^{(-)}(r)}{U_{2\nu}^{(-)}(s)}; \quad (4.21)$$

and in region III, $x > 0, h < r < 1$,

$$\begin{aligned} \psi(x, r) = & \frac{-i\Delta p(0)}{\rho_0(s)U_x(s)K_+^h(k^*(s))} \sum_{\nu=1}^{\infty} \frac{e^{i\alpha_{3\nu}^+ x} K_+^h(\alpha_{3\nu}^+) \text{Res}(1/K^h)|_{\alpha_{3\nu}^+}}{(\alpha_{3\nu}^+ - k^*(s))^2} \frac{U_{3\nu}^{(+)}(r)}{U_{3\nu}^{(+)}(s)} \\ & + \frac{-i\Delta p(0)}{\rho_0(s)U_x(s)K_+^h(k^*(s))} \text{Res}\left(\frac{e^{ikx} Q_{t,h}(r, k)}{(k - k^*(s))^2 K_-^h(k)}\right) \Big|_{k=k^*(s)}. \end{aligned} \quad (4.22)$$

The residue in the final term of (4.22) simplifies to

$$e^{ik^*(s)x} \left(\frac{iQ_{t,h}(r, k^*(s))x}{K_-^h(k^*(s))} + F(r, k^*(s)) \right), \quad (4.23)$$

where $F(r, k^*(s))$ is a complicated function which is independent of x . Equation (4.23) corresponds to a contribution with phase speed equal to the convected phase speed at $r = s$, and which is localized close to $r = s$ (as discussed following equation (4.15)). However, the linear x dependence of the amplitude of the first term in (4.23) means that this term contributes to the pressure field on $r = s$, despite having a convected phase there. In fact, its pressure is

$$-\frac{\Delta p(0)Q_{t,h}(r, k^*(s))e^{ik^*(s)x}}{K_-^h(k^*(s))} \quad (4.24)$$

for $r > s$ and $r < s$ respectively. This term evidently provides the appropriate pressure jump across $r = s$ to satisfy the Kutta condition at $x = 0$. Equation (3.4) is the $m = O(1)$ equivalent of (4.22) – note that the contributions from the nearly-convected spectrum S_c in (3.4) have combined to form the first term in the wake contribution (4.23) as

$m \rightarrow \infty$. Note also that equations (4.20)–(4.22) give the amplitudes of the scattered acoustic modes, and these amplitudes are all proportional to $\Delta p(0)$, the incident pressure jump at the trailing edge.

The second step in our scattering calculation is that we now find a correction to cancel the pressure jump $[\Delta p(x) - \Delta p(0)] e^{ik^*(s)x}$ across $r=s$ in $x > 0$. In order to do this we need a thin wake region, of width $O(1/|m|)$ around $r=s$, but of $O(1)$ extent in the axial direction. Using the inner radial coordinate $R = |m|(r-s)$, the leading-order momentum equations from (2.4) are

$$U_x \frac{\partial A_x}{\partial x} + U'_x A_r = -U'_x \left\{ x k_r^* i \phi + |m| \frac{\partial \phi}{\partial R} \right\}, \quad (4.25)$$

$$U_x \frac{\partial A_r}{\partial x} - 2 \frac{U_\theta}{s} A_\theta = \left\{ m \frac{(rU_\theta)'}{s^2} + k^* U'_x \right\} i \phi, \quad (4.26)$$

$$U_x \frac{\partial A_\theta}{\partial x} + \frac{(rU_\theta)'}{s} A_r = -\frac{(rU_\theta)'}{s} \left\{ x k_r^* i \phi + |m| \frac{\partial \phi}{\partial R} \right\}, \quad (4.27)$$

in which k^* and all mean flow quantities are evaluated at $r=s$, and k_r^* is the r -derivative of $k^*(r)$, also evaluated at $r=s$. Equations (4.25)–(4.27) are equivalent to equations (26)–(28) in Cooper & Peake (2005). The leading-order continuity equation, (2.5), becomes

$$m^2 \left[\frac{\partial^2 \tilde{\phi}}{\partial R^2} - \left(\left(\frac{k^*}{m} \right)^2 + \frac{1}{s^2} \right) \tilde{\phi} \right] e^{-iR x k_r^*/|m|} = -|m| \frac{\partial A_r}{\partial R} - i x k_r^* A_r - \frac{i m}{s} A_\theta - i k^* A_x, \quad (4.28)$$

where $\tilde{\phi} \equiv \phi e^{iR k_r^*(s)x/|m|}$ and k^* , k_r^* and all mean flow quantities are again evaluated at $r=s$. Equation (4.28) is the equivalent of equation (29) in Cooper & Peake (2005).

Equations (4.25)–(4.28) are solved in R positive and R negative separately, with matching conditions that the radial velocity, $A_r + \partial \phi / \partial R$, is continuous across $R=0$, while the pressure jumps by $-[\Delta p(x) - \Delta p(0)] e^{ik^*(s)x}$ across $R=0$. The outer boundary conditions are that $A_x, A_r, A_\theta, \phi \rightarrow 0$ as $R \rightarrow \pm \infty$. The system is marched downstream from $x=0$, with initial conditions $A_{x,r,\theta} = \phi = 0$. A simple Euler routine for (4.25)–(4.27) is used to march in x . At each x station, the Green's function for (4.28) can easily be found analytically, which provides a particular integral in terms of A evaluated at the previous x station. The particular integral decays as $R \rightarrow \pm \infty$, and the complementary solutions are adjusted to satisfy the velocity and pressure conditions at $R=0$. In this way the wake correction term can be calculated for arbitrary $x > 0$; given the use of the inner radial scaling, it is localized around $r=s$. Note that, although we have forced the unsteady pressure and the radial component of unsteady velocity to be continuous across $r=s$, the axial and azimuthal components of unsteady velocity in (4.23) and in this latest correction term are not continuous across $r=s$. This discontinuity is the wake sheet of this particular problem, which exists downstream of the trailing edge and at the convected wavelength.

We have now determined the total unsteady field as the sum of the incident disturbance and its wall boundary layers, the scattered sonic field from the inner region and the wake term described in the previous paragraph. Figure 9 shows the total unsteady pressure field. The incident disturbance arrives from upstream outboard of the splitter, and the requirements of continuous pressure in the fluid and the imposition of the Kutta condition at the trailing edge produce the scattering shown. For these parameter values we find 2, 12 and 12 cut-on sonic modes present in regions I, II and III respectively, of which 1, 6 and 6 are downstream-travelling. In addition to these sonic modes there is an infinite spectrum of nearly-convected modes and a

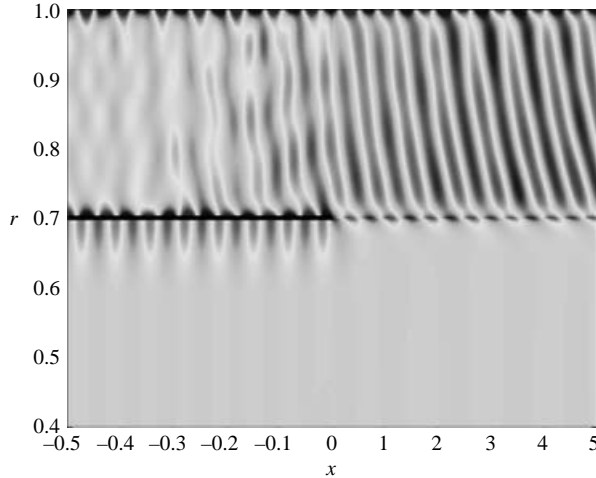


FIGURE 9. The total unsteady pressure field for the scattering of the nearly-convected disturbance at the trailing edge. The incident disturbance arrives from upstream in $r \geq 0.7$. Conditions as in figure 8.

continuous spectrum, which contribute to the pressure and which are represented in our asymptotic regime by the hydrodynamic terms in the scattered field. The incident convected disturbance in the body of the flow, and its boundary layer on the outer wall, continue downstream largely unaffected by the splitter, exactly as in figure 8. The immediate vicinity of the trailing edge produces the acoustic response of cut-on modes in all three regions. The presence of sonic modes propagating downstream in region III, and upstream in region II, can be seen from the distortion of the incident phase fronts of figure 8. In region I only sonic modes are present. Downstream of the trailing edge there is a shed wake sheet on $r = s$, across which the tangential (axial and azimuthal) disturbance velocities are discontinuous, but normal (radial) velocities and the pressure in the fluid are continuous.

This overall picture of scattering driven by conditions on the pressure contrasts with the uniform mean flow scenario. In the absence of mean vorticity the convected disturbance has no associated pressure, and as a result would convect past the trailing edge silently. However, the presence of mean vorticity means that the incident hydrodynamic disturbance induces a pressure jump across the plate, so that acoustic modes are scattered from the trailing edge to enforce the Kutta condition.

A final remark on the results of this section is that the large- $|m|$ scattering solutions in the four configurations (sonic or nearly-convected incident disturbance at leading or trailing edge) can be combined to obtain the solution for a splitter of finite length. For disturbances of asymptotically short wavelength the solution for a finite splitter involves only repeated reflection and transmission of the propagating (the cut-on sonic and the nearly-convected) modes at the two ends of the splitter, which is easily performed using the results of the present analysis.

5. Concluding remarks

We mention first the energy balance of our system. The energy equation is

$$\frac{\partial E}{\partial t} + \nabla \cdot \mathbf{I} = \mathbf{u}' \cdot \left(\mathbf{U}_0 \wedge \left[\rho_0 \boldsymbol{\xi}' - \frac{p'}{c_0^2} \boldsymbol{\xi}_0 \right] \right) \quad (5.1)$$

where $\boldsymbol{\xi}' = \nabla \wedge \mathbf{u}$ is the disturbance vorticity,

$$E = \frac{p'^2}{2\rho_0 c_0^2} + \frac{\rho_0 \mathbf{u}'^2}{2} + \frac{p'}{c_0^2} \mathbf{u}' \cdot \mathbf{U}_0 \quad (5.2)$$

is the energy density and

$$\mathbf{I} = \left(\frac{p'}{\rho_0} + \mathbf{u}' \cdot \mathbf{U}_0 \right) \left(\rho_0 \mathbf{u}' + \frac{p'}{c_0^2} \mathbf{U}_0 \right) \quad (5.3)$$

is the energy flux vector. Equation (5.1) is the appropriate special case of the energy equation (1.87) of Goldstein (1976), i.e. for isentropic perturbations on a homentropic flow and with no external volume sources of mass or momentum. Note that (5.1) has source terms on the right-hand side as a direct consequence of the flow (mean and unsteady) vorticity. The actual calculation of (say) the time-averaged axial energy flux is complicated by the presence of mean vorticity, because the eigenvalue problem is not self-adjoint and the modes are not orthogonal to each other. Let \mathbf{B} be the vector of mode amplitudes in a duct, as for instance in (2.30), then the time-averaged axial energy flux down the duct is

$$\left\langle \int I_x r \, dr \, d\theta \right\rangle = \frac{1}{2} \text{Re} \sum_{\mu, \nu} \mathbf{M}_{\mu\nu} B_\mu B_\nu^* e^{i(\alpha_\mu - \alpha_\nu^*)x}. \quad (5.4)$$

In (5.4) the angle brackets denote time average, and $\mathbf{M}_{\mu\nu}$ is the matrix of the inner products of the μ th and ν th modes. In the absence of swirl the modes are orthogonal and $\mathbf{M}_{\mu\nu}$ is diagonal, but that is not true here and the off-diagonal contributions must be included. For each of our problems we have computed the time-averaged axial energy flux at $x=0_\pm$ using (5.4), including the contributions of the cut-off sonic modes as these only decay far away from $x=0$. The axial energy flux has been verified to be continuous across $x=0$ in each case, which provides a useful check on the mutual consistency of the solutions in the various regions.

In this paper we have considered two distinct regimes, namely $O(1)$ azimuthal mode number, in which an exact solution has been presented for a specialized mean flow (§2 and §3), and large azimuthal mode number, in which simplification and generalization of this exact solution has been possible (§4). A number of comparisons between the two regimes can be made:

(a) In both regimes an incident *sonic* disturbance scatters predominantly into sonic modes, at both a leading and a trailing edge. The physics of this situation is very similar to the scattering of acoustic waves in irrotational mean flow, with mode selection in the scattered field depending in part on both the proximity of the incident and scattered wavenumbers in the k -plane and on the spatial match between the corresponding eigenfunctions. At a leading edge, scattered vortical hydrodynamic disturbances (i.e. nearly-convected modes) are produced when $m = O(1)$, which make a small contribution to the unsteady pressure. This is in contrast to the case of irrotational mean flow, where no extra vorticity is generated at the leading edge.

(b) At a leading edge the scattering of a *nearly-convected* disturbance shows some differences between the two regimes. In the large- m case the scattered sonic field dominates in the total unsteady pressure over all other terms (including over the incident pressure field). In contrast, the results shown in figure 4 suggest that for $m = O(1)$ the nearly-convected scattered modes carry at least as much scattered pressure as the sonic modes.

(c) For the scattering of nearly-convected disturbances at a *trailing* edge, then for both $m = O(1)$ and $m \gg 1$ a sonic scattered field is produced whose magnitude is proportional to the pressure jump of the incident field at the trailing edge. This apparently general behaviour in a swirling flow contrasts with the case of irrotational mean flow. Because the vorticity waves in an irrotational mean flow are pressure-free, they need not scatter at a trailing edge to enforce a Kutta condition, and rather just continue downstream into the wake. The production of a sonic field here is a qualitatively different response.

One feature of rigid-body swirl with uniform axial flow is that it does not possess a continuous spectrum of axial wavenumbers, which has allowed a number of simplifications (including that the Wiener–Hopf function $K(k)$ is meromorphic, so that the infinite-product factorization can be used). In contrast, for $m \gg 1$ we were able to complete an asymptotic analysis for arbitrary mean flows, with the continuous spectrum, if present, being implicitly included within the down-marching of the nearly-convected flow (equation (4.6)). Work on the continuous spectrum for $m = O(1)$ is in progress.

The authors are very grateful to Dr M. E. Goldstein for pointing out the analytical solution to (4.6) which is given in Appendix B, and Dr A. J. Cooper for providing computed data for the incident gust used in §4.4.

Appendix A

In this appendix we present two methods used to factorize the Wiener–Hopf kernel (2.29) in the form $K(k) = K_+(k)K_-(k)$ with $K_\pm(k)$ analytic, non-zero and with algebraic behaviour at infinity in the upper and lower halves of the complex- k -plane respectively.

First, using the methods and results in Noble (1958), $K_\pm(k)$ are given via the explicit integral formula

$$K_\pm(k) = \exp\left(\frac{\pm 1}{2\pi i} \int_{\Gamma_\pm} \frac{\log K(\xi)}{\xi - k} d\xi\right), \tag{A 1}$$

where the contours Γ_\pm run from $-\infty$ to $+\infty$ along the boundaries, $\text{Im}(k) = \mp \delta$, of the overlapping upper and lower half-planes respectively. Evaluating (A 1) numerically requires a little care, as the convergence of the integrals at $\pm\infty$ is slow and needs to be monitored. Also, when the fictitious dissipation of the Wiener–Hopf technique is set to zero all the nearly-convected and cut-on sonic modes give poles on the real axis, and one must deform the integration contours away from all these poles to facilitate accurate numerical integration.

Second, as an alternative factorization method, since $K(k)$ is meromorphic it can also be decomposed via infinite products. This method gives more insight into the structure of $K_\pm(k)$, and provides an important check of the accuracy of the numerical factorization (A 1). The poles and zeroes of the kernel function $K(k)$ are the eigenvalues in regions I, II and III, and we can immediately write

$$K_\pm(k) = \frac{\sqrt{K(0)} e^{\frac{1}{2}kK'(0)/K(0)} e^{\pm\chi(k)} \left(\prod_\mu (1 - k/\alpha_{3\mu}^\mp) e^{k/\alpha_{3\mu}^\mp}\right)}{\left(\prod_\mu (1 - k/\alpha_{1\mu}^\mp) e^{k/\alpha_{1\mu}^\mp}\right) \left(\prod_\mu (1 - k/\alpha_{2\mu}^\mp) e^{k/\alpha_{2\mu}^\mp}\right)}, \tag{A 2}$$

where the wavenumbers $\alpha_{1\mu,2\mu,3\mu}^\pm$ are eigenvalues corresponding to regions I, II and III respectively. For $K_+(k)$ the product is taken over all modes with label $\mu \in S_a^-$, and for $K_-(k)$ the product is taken over all modes with label $\mu \in S_a^+ \cup S_c$. Note that all the nearly-convected modes lie in the UHP and so are not present in the formula for $K_+(k)$. In (A 2) the exponential factors $e^{k/\alpha}$ are necessary to ensure convergence of the products and the factor $e^{\frac{1}{2}kK'(0)/K(0)}$ ensures that $K_\pm(k)$ have the correct behaviour for small k , see Noble (1958, p. 40) for full details.

The exponential term involving $\chi(k)$ is included in (A 2) so as to guarantee that the factors behave algebraically at infinity. Using the methods on p. 128 of Noble (1958), we find that to cancel the exponential behaviour of $K_+(k)$ as $k \rightarrow \infty$ in the UHP,

$$\begin{aligned} \chi(k) + \frac{1}{2}k \frac{K'(0)}{K(0)} &= k \left(\frac{\log a}{a} - \frac{\log e}{e} - \frac{\log c}{c} \right) \\ &+ k \left(\sum_{\mu=1}^{\infty} \left(\frac{1}{\alpha_{3\mu}} + \frac{1}{a\mu} \right) - \sum_{\mu=1}^{\infty} \left(\frac{1}{\alpha_{1\mu}} + \frac{1}{c\mu} \right) - \sum_{\mu=1}^{\infty} \left(\frac{1}{\alpha_{2\mu}} + \frac{1}{e\mu} \right) \right). \end{aligned} \quad (\text{A } 3)$$

Here the coefficients a , e and c refer to the large-order behaviour of the cut-off acoustic modes; specifically, a is given by (2.15) with $\sigma = h$, $t = 1$; c with $\sigma = h$, $t = s$; and e with $\sigma = s$, $t = 1$. With this choice of $\chi(k)$, the behaviour of $K_-(k)$ in the LHP will also be algebraic.

Finally, we can determine the algebraic behaviour of the factors at infinity by noting that as $k \rightarrow \infty$

$$K(k) \sim (\mathcal{C}|k|\Lambda(k))^{-1}, \quad (\text{A } 4)$$

where $\mathcal{C} = -\frac{1}{2}\sqrt{1 - U^2/c_0^2(s)}$. The function $|k|$ is written as the product of factors $(k \pm i\epsilon)^{1/2}$, which have branch cuts to infinity running along the negative and positive imaginary axes respectively, and which are analytic and non-zero in the upper and lower halves of the complex- k -plane respectively. The factor $\Lambda(k)$ in (A 4) has a single zero at $k = k_c$, which corresponds to pure convection and lies in the upper half-plane. Putting this information together, we see that $K_+(k) \propto k^{-1/2}$ and $K_-(k) \propto k^{-3/2}$ as $k \rightarrow \infty$.

Appendix B

The system of equations (4.6) was originally presented as equations (16)–(19) in Cooper & Peake (2005). In this Appendix we give an analytical solution due to M. E. Goldstein (private communication, 2005). In the notation of §4 the full equations are

$$U_x \frac{\partial A_x}{\partial x} + \frac{dU_x}{dr} A_r = -\frac{dU_x}{dr} \frac{dk^*}{dr} i_x \Phi, \quad (\text{B } 1)$$

$$U_x \frac{\partial A_r}{\partial x} - 2\frac{U_\theta}{r} A_\theta = \left\{ \frac{m\Gamma}{r} + k^* \frac{dU_x}{dr} \right\} i \Phi, \quad (\text{B } 2)$$

$$U_x \frac{\partial A_\theta}{\partial x} + \Gamma A_r = -\Gamma \frac{dk^*}{dr} i_x \Phi, \quad (\text{B } 3)$$

$$\lambda^2 \Phi = i \left\{ x \frac{dk^*}{dr} A_r + \frac{m}{r} A_\theta + k^* A_x \right\}, \quad (\text{B } 4)$$

where $\Gamma = (1/r) d(rU_\theta)/dr$, and $\lambda^2 = x^2 (dk^*/dr)^2 + \frac{m^2}{r^2} + k^{*2}$. Note that r appears only as a parameter in these equations.

To proceed we define the new variable

$$Y = \frac{m}{r} A_\theta + k^* A_x, \quad (\text{B } 5)$$

and combining (B 1), (B 2), (B 4) one obtains the following equation:

$$\lambda^2 U_x \frac{\partial}{\partial x} \left[\left(\frac{\Gamma m}{r} + k^* \frac{dU_x}{dr} \right) A_\theta - \Gamma Y \right] = 0, \quad (\text{B } 6)$$

and hence

$$A_\theta = \frac{\Gamma Y}{(\Gamma m/r + k^* dU_x/dr)} + f(r), \quad (\text{B } 7)$$

where $f(r)$ is an arbitrary function of radius determined by initial conditions. Now substituting (B 7) into (B 2), and using (B 1), (B 2), (B 4) to eliminate A_r yields, after some considerable manipulation,

$$U_x^2 \lambda^2 \frac{\partial^2 Y}{\partial x^2} + 2U_x^2 x \left(\frac{dk^*}{dr} \right)^2 \frac{\partial Y}{\partial x} - \left[\left(U_x \frac{dk^*}{dr} + \frac{\Gamma m}{r} + k^* \frac{dU_x}{dr} \right) \left(\frac{\Gamma m}{r} + k^* \frac{dU_x}{dr} \right) - 2 \frac{U_\theta}{r} \Gamma \left(\frac{m^2}{r^2} + k^{*2} \right) \right] Y = -2 \frac{U_\theta}{r} \left(\frac{m^2}{r^2} + k^{*2} \right) \left(\frac{\Gamma m}{r} + k^* \frac{dU_x}{dr} \right) f(r). \quad (\text{B } 8)$$

We now introduce the new independent variable

$$y = ix \frac{dk^*}{dr} \left(\frac{m^2}{r^2} + k^{*2} \right)^{-1/2}, \quad (\text{B } 9)$$

for which (B 8) becomes

$$(1 - y^2)Y'' - 2Y' + C(r)Y = F(r), \quad (\text{B } 10)$$

where a prime now denotes a derivative with respect to y . Equation (B 10) is Legendre's equation in the variable y , the coefficient $C(r)$ is given by

$$C(r) = \frac{1}{U_x^2 (dk^*/dr)^2} \left[\left(U_x \frac{dk^*}{dr} + \frac{\Gamma m}{r} + k^* \frac{dU_x}{dr} \right) \left(\frac{\Gamma m}{r} + k^* \frac{dU_x}{dr} \right) - 2 \frac{U_\theta}{r} \Gamma \left(\frac{m^2}{r^2} + k^{*2} \right) \right], \quad (\text{B } 11)$$

and

$$F(r) = \frac{2U_\theta}{U_x^2 (dk^*/dr)^2 r} \left(\frac{m^2}{r^2} + k^{*2} \right) \left(\frac{\Gamma m}{r} + k^* \frac{dU_x}{dr} \right) f(r). \quad (\text{B } 12)$$

The general solution for $Y(y, r)$, from which $A(x, r)$ and $\Phi(x, r)$ can be deduced, is therefore

$$Y(y, r) = \frac{F(r)}{C(r)} + \alpha(r) P_\nu^0(y) + \beta(r) Q_\nu^0(y), \quad (\text{B } 13)$$

for some $\alpha(r)$ and $\beta(r)$, where $\nu = \nu(r)$ is a root of $\nu(\nu + 1) = C(r)$ and P_ν^μ, Q_ν^μ are the associated Legendre functions of the first and second kind.

REFERENCES

- BENDER, C. M. & ORSZAG, S. A. 1978 *Advanced Mathematical Methods for Scientists and Engineers*. McGraw-Hill.
- CHAPMAN, C. J. 1994 Sound radiation from a cylindrical duct. Part 1. Ray structure of the duct modes and of the external field. *J. Fluid Mech.* **281**, 293–311.

- COOPER, A. J. & PEAKE, N. 2005 Upstream-radiated rotor-stator interaction noise in mean swirling flow. *J. Fluid Mech.* **523**, 219–250.
- CRIGHTON, D. G. 1985 The Kutta condition in unsteady flow. *Annu. Rev. Fluid Mech.* **17**, 411–445.
- GOLDSTEIN, M. E. 1976 *Aeroacoustics*. McGraw-Hill.
- GOLDSTEIN, M. E. 1978a Characteristics of the unsteady motion on transversely sheared mean flows. *J. Fluid Mech.* **84**, 305–329.
- GOLDSTEIN, M. E. 1978b Unsteady vortical and entropic distortions of potential flows round arbitrary obstacles. *J. Fluid Mech.* **89**, 433–468.
- GOLDSTEIN, M. E. 1979 Scattering and distortion of the unsteady motion on transversely sheared mean flows. *J. Fluid Mech.* **91**, 601–632.
- GOLUBEV, V. V. & ATASSI, H. M. 1998 Acoustic-vorticity waves in swirling flows. *J. Sound Vib.* **209**, 203–222.
- GOLUBEV, V. V. & ATASSI, H. M. 2000 Unsteady swirling flows in annular cascades, Part 1: Evolution of incident disturbances. *AIAA J.* **38**, 1142–1149.
- HARDY, G. H. 1963 *A Course of Pure Mathematics*. Cambridge University Press.
- HOWE, M. S. 1986 Attenuation of sound due to vortex shedding from a splitter plate in a mean flow duct. *J. Sound Vib.* **105**, 385–396.
- KERREBROCK, J. L. 1977 Small disturbances in turbomachine annuli with swirl. *AIAA J.* **15**, 794–803.
- LALAS, D. P. 1975 The ‘Richardson’ criterion for compressible swirling flows. *J. Fluid Mech.* **69**, 65–72.
- MAHMOUD-UL-HASSAN & RAWLINS, A. D. 1998 Two problems of waveguides carrying mean fluid flow. *J. Sound Vib.* **216**, 713–738.
- MAHMOUD-UL-HASSAN & RAWLINS, A. D. 1999 Sound radiation in a planar trifurcated lined duct. *Wave Motion* **29**, 157–174.
- NIJBOER, R. J. 2003 Sound diffraction by the splitter in a turbofan rotor-stator gap swirling flow. *Tenth Intl Conf. on Sound and Vibration, Stockholm 2003* (ed. A. Nilsson & H. Boden). International Institute of Acoustics & Vibration.
- NIJBOER, R. J. & SIJTSMA, P. 1998 Theory of splitter diffraction in annular ducts. *NLR paper NLR-TR-98525*.
- NOBLE, B. 1958 *Methods Based on the Wiener–Hopf Technique for the Solution of Partial Differential Equations*. Pergamon.
- RAWLINS, A. D. 1995 A bifurcated circular waveguide problem. *IMA J. Appl. Maths* **54**, 58–81.
- RIENSTRA, S. W. 1984 Acoustic radiation from a semi-infinite duct in a uniform subsonic mean flow. *J. Sound Vib.* **94**, 267–288.
- TAM, C. K. W. & AURIAULT, L. 1998 The wave modes in ducted swirling flows. *J. Fluid Mech.* **371**, 1–20.
- YAKUBOV, S. 1994 *Completeness of Root Functions of Regular Differential Operators*. Harlow.